The Strain-based Approach to Predict the Initiation and Propagation of the Crack for the Vintage Pipeline Materials Using the Extended Finite Element Method (XFEM)

by

Nahid Elyasi

A thesis submitted in partial fulfillment of the requirements for the degree of

Master of Science

Department of Mechanical Engineering
University of Alberta

Abstract

Vintage pipelines are widely used in the transmission of gas and oil in North America. They are subject to varieties of loading conditions, especially in aggressive environments in arctic region. Displacement-controlled loads lead to severe longitudinal plastic strain and consequently failure in pipelines. Strain-based design (SBD) can be an effective and economical method in designing pipelines under severe plastic strain.

The goal of the current study was to investigate the efficiency of strain-based damage criteria using the extended finite element method (XFEM) to predict the initiation and propagation of the crack in two specific grades of vintage pipelines.

First, the damage criteria, maximum principal strain (Maxpe), and fracture energy (G_c) were obtained for the X52 vintage pipeline under internal pressure and eccentric tension loading using XFEM analysis in the ABAQUS software. Then, the predicted XFEM results were validated with previously published eight full-scale experimental tests, and tensile strain capacity (TSC) for each model was calculated.

In the second step, to investigate the capability of the strain-based XFEM analysis in the prediction of small-scale tests as well, the initiation and propagation of the crack in the single edge notched tension (SENT) test was simulated. The strain-based damage parameters were applied in the SENT model of vintage X42 grade of pipeline and XFEM results were validated with experiments.
The current research investigated the reliability of strain-based damage parameters in the prediction of fracture response in X42 and X52 grades of the vintage pipeline using XFEM. The

results showed the capability of the XFEM tool to predict the damage response in both full-scale

and small-scale models for these grades of the vintage pipeline.

Preface

All the research work presented for this thesis forms part of a research collaboration between the University of Alberta and Enbridge Liquid Pipelines Ltd., with Dr. Westover and Professor Adeeb being the lead collaborator at the University of Alberta and Nader Yoosef-Ghodsi being responsible for acquisition of research funding at Enbridge.

A version of Chapter 3 of this dissertation has been published as N. Elyasi, M.M. Shahzamanian, M. Lin, L. Westover, Y. Li, M. Kainat, N. Yoosef-Ghodsi, S. Adeeb, Prediction of Tensile Strain Capacity for X52 Steel Pipeline Materials Using the Extended Finite Element Method, Appl. Mech. 2 (2021) 209–225. I was responsible for the study design, data extraction and analysis as well as the manuscript composition. L. Westover and S. Adeeb were the supervisory authors and were involved with conceptualization, analysis and manuscript edits. M. Kainat, and N. Yoosef-Ghodsi assisted in funding acquisition, M.M. Shahzamanian was the supervisory author and assisted in reviewing the manuscript. Y. Li and M. Lin assisted in reviewing the manuscript.

N. Elyasi

Dedication

This work is dedicated to my only brother, **Mohammad Mahdi Elyasi,** an ethereal passenger of flight PS752.

Acknowledgments

My deepest gratitude goes to my supervisors, Dr. Lindsey Westover and Prof. Samer Adeeb for their endless support and motivation. Without their guidance and constant feedback this MSc would not have been achievable.

Table of Contents

List of Tables

List of Figures

Chapter 1: Introduction

1.1 Background and motivation

Pipelines are considered to be the most economical method for transportation of natural gas and oil over long distances [1]. To transport the energy from the source to target locations, long distance pipeline networks traverse regions with different soil and geological conditions (Figure 1.1) [1]. In harsh environments, characterised by extreme temperature variations and large ground movements, the pressurised pipelines may develop large longitudinal plastic strains. The large longitudinal deformations in onshore pipelines occur as a result of ground movements due to slope instability, seismic activity, and frost heave. Large deformations happen in offshore pipelines when girth welded parts of the pipelines are wound to a spool, causing high bending strains. Also, flaws in girth weld can cause excessive tensile strains in the pipeline. All of these situations cause the failure of pipes as a result of high strain levels and represent significant threats to the integrity of pipelines [2].

Traditional stress-based designs are not economical in designing pipelines under large plastic strains [3] because it uses the minimum yield stress of the pipe as the failure condition. On the other hand, the strain-based design (SBD) criterion is based on displacement controlled loading and limit state design. Under displacement loading, pipeline longitudinal strain is allowed to exceed the pipeline yield strain. Although in such loading conditions, the pipeline is subjected to some plastic strains, it still satisfies the operation safety requirements and is able to tolerate the excess deformation over the yield. The SBD approach can therefore be supplementary to a stress-based design criterion and it improves the pipeline's capability to satisfy the operation requirements, resulting in economic and secure designs [4].

Figure 1.1 The trans-Alaska oil pipeline crosses the landscape [1].

The recent studies mostly investigated the fracture properties of high grades pipeline steel (X60 and above), while limited research focused on vintage low-grade pipelines [5]. On the other hand, a significant percentage of pipelines used in transmission energy in North America are vintage pipelines [6]. It shows the importance of the development of SBD for vintage pipelines subjected to large plastic strain in such a harsh environment.

1.2 Objectives

The main objective of this research is to predict the crack initiation and propagation of two specific grades of the vintage pipeline (X42 and X52)

1.2.1 Specific objectives

The following are the specific objectives (SO) of the research:

i. Extensive literature search to obtain results of tests conducted using small-scale samples of X42 grade and full-scale samples of X52 grade of pipeline steels

ii. Calibrate and validate XFEM models of the two vintage grades of the pipes using their respective test data

iii. Assess the effect of varying (maximum principal strain, fracture energy, mesh size, crack extension criteria) on accurate prediction of fracture strength

iv. Assess the correlation between the set of data used in modelling and resulting fracture strength.

SO 1: For the X52 grade of the vintage pipeline, the XFEM-based model of the full-scale test will be developed and damage properties obtained and then used to calculate the tensile strain capacity of this grade of pipelines.

SO 2: For the X42 grade of the vintage pipeline, the XFEM-based model of the small-scale test will be developed and fracture response will be obtained and compared with experimental results. Finally, the correlation between fracture response in the small-scale and full-scale approach using the same damage parameters will be discussed.

1.3 Thesis outline

The research is organized into five chapters as follows:

Chapter 1 provides an introduction, a brief background and motivation of the research.

Chapter 2 covers the necessary background literature on selective topics in pipelines, including vintage pipelines, fracture mechanics as well as the theoretical approach of XFEM.

Chapter 3 presents the XFEM modelling of the X52 grade of pipeline. The analysis used to predict the damage parameters of the pipe model under internal pressure and external loading. The XFEM results of the proposed model are compared with experiments and the TSCs of the X52 vintage pipeline are calculated.

Chapter 4 presents the XFEM modelling of Single Edge Notch Tension (SENT) tests to predict the crack initiation and propagation parameters of the X42 vintage pipeline. The XFEM models of the X42 pipes is used to predict the tensile strain capacity of the pipe and the results compared with test results.

Chapter 5 summarizes the results of this research and presents recommendations for future work.

Chapter 2: Literature Review

2.1 Introduction of pipelines

2.1.1 Evolution of the pipe grades

Vintage pipeline steels (e.g. X46, X52, and X56 pipelines) were manufactured from relatively low yield strength steels and old construction techniques in the early 1960s [7,8]. Although vintage pipelines with normal strength such as X60, X65, and X70 were introduced in the 1970s, they were not widely used in pipeline construction due to restrictions in the welding technology [7]. However, thermomechanical treatment strengthened the weldability of these grades of pipeline and prepared the way for the manufacturing process of the modern high strength pipelines. Although modern high strength pipelines such as X80, X100, and X120 are currently being produced, still there is a limitation in utilizing them in pipeline construction due to a lack of data on their load response history. On the other hand, vintage pipes have high ductility and can safely undergo large strain under applied load due to differential ground movement [9,10].

The vintage steel pipes were manufactured before the 1990s. They have higher carbon content and manufacturers put micro-alloying elements to strengthen their microstructure. The higher carbon content in the form of pearlite increases the strength but causes welding difficulties in comparison to modern steel pipes with lower carbon content [11]. It can be observed from the microstructure of the vintage pipeline steel that ferrite and pearlite are the majority. On the other hand, modern steels have ferrite and bainite and contain a lower level of carbon [12,13]. Thermomechanical controlled processes produce the higher strength microstructure containing an acicular ferrite and bainite in modern pipelines instead of the structure with ferrite and pearlite observed in the vintage pipelines [14]. The microstructure of the vintage X52 pipeline with a high

carbon level is shown in Figure 2.1 and compared with the new X52 grade of pipelines [15]. The observations show almost 70 % volume fraction of vintage X52 pipe contain ferrite, and 30% pearlite, which can be observed as the light and dark colored parts in Figure 2.1, respectively [15]. On the other hand, the microstructure of the new X52 pipe mostly contains acicular and polygonal ferrite. Also, it can be seen that vintage X52 has a coarser grain size in comparison with new X52, which causes higher resistance to hydrogen attack in new X52 grade of pipelines [15]. Although the high percentage of carbon in the vintage pipelines caused higher fatigue resistance, it resulted in welding difficulties. Therefore, the high percentage of carbon is not used in modern pipelines [15].
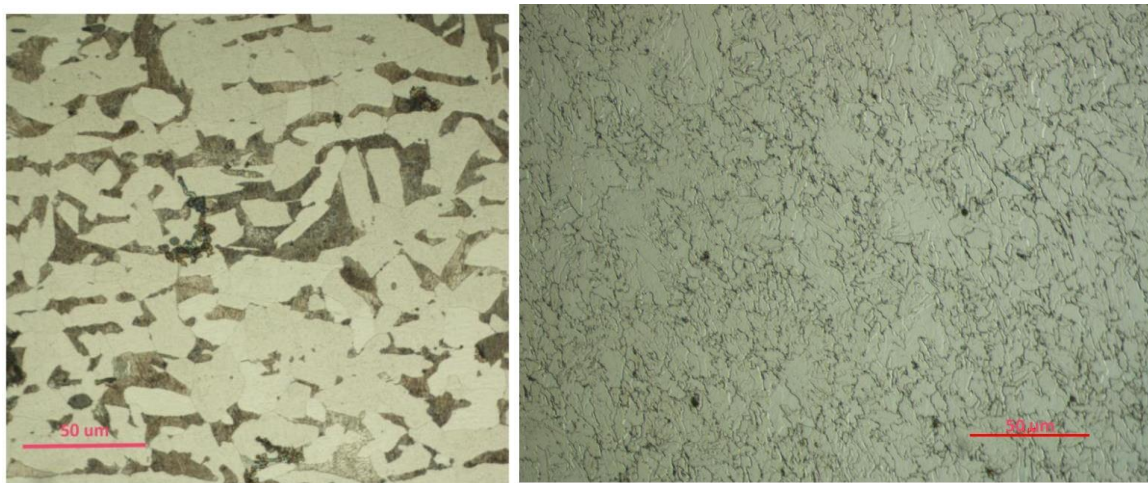
(a)   (b)

Figure 2.1 Microstructure of (a) vintage X52 alloy contains ferrite and pearlite and (b) new X52 alloy (scale bars 50 μm) [15].

2.1.2   Failure of pipelines

Pressurized onshore steel pipelines are usually buried underground. So, they are susceptible to threats caused by both external loadings and internal pressure. The external loadings like

displacements and loads from geotechnical instabilities lead to bending strains and stresses and substantial axial tension on pipelines [16].

Failure in pressurized pipelines mainly happened when the stress in the pipe wall surpasses a critical failure value and is observed in the pipeline as leakage or rupture. External bending forces due to soil movements typically cause circumferential cracks in pipeline. It typically occurs in pipes with a small diameter and the crack can fully or partially propagate around the pipe's circumference [16].

Failure happens not only on the base metal of the pipes but may also occur at the joints like girth welds. Girth weld flaws are the potential threats in welded pipelines as inappropriate joint connection can lead to leakage through the welded joints, especially at high operation systems [17].

2.2 Fracture

2.2.1 Characterization of fracture

The term fracture can be described as the separation of a solid body under applied stress. The general process of a fracture can be described by the crack formation followed by the crack propagation [18]. Figure 2.2 shows the different stages of the creation of cup-and-cone fracture in a ductile specimen such as X52 and X42 steel vintage pipelines under uniaxial tensile stress. First, ductile fracture begins with the nucleation and growth of micro voids in the interior of the test bar. Then, by increasing the local stress, the micro voids grow and coalesce into larger cavities to form an internal crack. The crack grows outward vertical to the tension stress into larger cracks and then propagates rapidly to the edge of the test bar at 45° to the tensile stress. Finally, shear lips are

formed due to shear stress around the periphery of the neck, giving the final fracture surface the cup and cone shape (Figure 2.2) [19,20].

2.2.2 Fracture mechanics

Anderson [21] and Czichos et al. [22] identified and described the fracture mechanics design approach (FMDA) and the traditional design approach (TDA) for the selection of materials and structural design. The traditional design approach focuses on the strength of materials. Both tensile and yield strength of the material are usually obtained in a tension test to determine the resistance of the material to applied tension force.
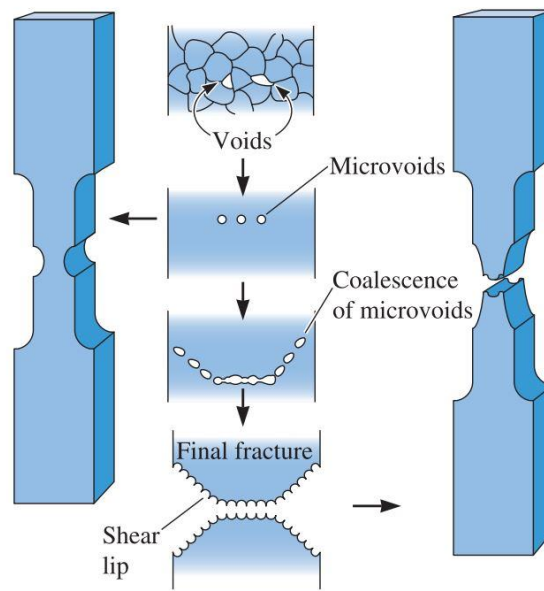
Figure 2.2 The sequence of formation of tensile fracture in ductile steel specimen [19]

In the fracture mechanics approach the crack size was added as a new parameter and the fracture toughness of the material is measured instead of its tensile properties. The fracture toughness calculates the material's resistance to the formation and propagation of the crack. It can be

8

calculated directly using a fracture toughness test or indirectly using a Charpy V-notch (CVN) impact test to predict the required fracture energy of the notched specimen [16]. It is important to prefabricate a notch or crack to produce the extreme condition and stress concentration near the tip of the crack to measure the material's fracture toughness [23].

However, the fracture mechanics approach aims to determine the stress and strain fields near the crack tip using a single toughness parameter, such as the stress-intensity factor (K). The crack growth begins when the stresses near the crack tip reach the fracture toughness of the material, which is defined by the stress-intensity factor [21].

The stress distribution at the crack tip can be broken up into three components, according to the modes of fracture, namely Mode I, Mode II, and Mode III, as sketched in Figure 2.3. For these basic fracture modes, the stress intensity factor is written as K_I (for Mode I), K_{II} (for Mode II), and K_{III} (for Mode III), with subscript in Roman numbers [24]. The stress-intensity factor is a function of the size of the crack, the applied stress, and the effect of the specimen geometry constraint. Anderson [21] and Czichos et al. [22] generally expressed the stress intensity factor (K) as follows:

$$K_{I,\ II,\ III} = Y\sigma\sqrt{\pi a} \qquad\qquad\qquad 2.1$$

where $K_{I,\ II,\ III}$ is the stress intensity factor related to each fracture mode (MPa$\sqrt{m}$), σ is the characteristic stress (MPa), a is the characteristic crack dimension (m), and Y is a dimensionless constant that depends on the mode of loading and the geometry of the specimen.

The three fracture modes defined according to the applied loading condition at the crack surfaces are presented in Figure 2.3 and described as follows:

9
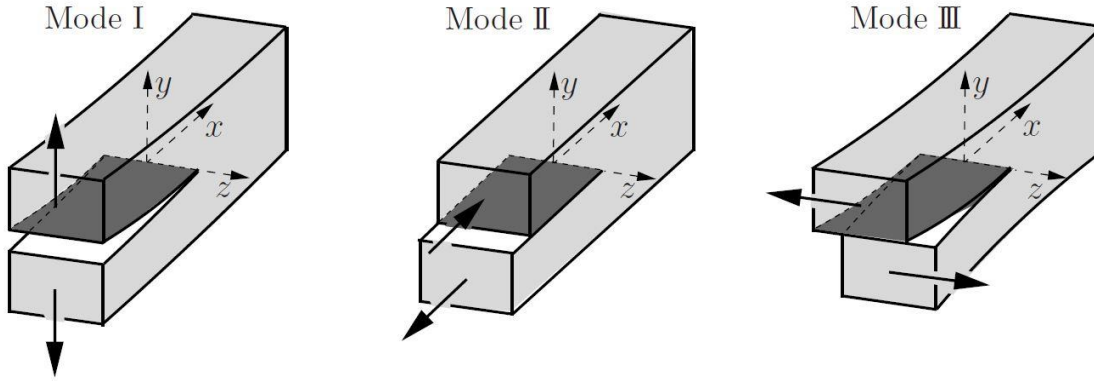
Figure 2.3 The three basic modes of fracture: Mode I (opening), Mode II (In-Plane Shear), and Mode III

(Out-of-Plane Shear) [25].

Mode I (Opening mode): The crack opens orthogonal to the local fracture surface. In this mode, the applied tensile stress is normal to the crack surface.

Mode II (In-plane shear mode): The crack surfaces slide relatively to each other normal to the crack front and cause shear stress which is parallel to the crack surface.

Mode III (Out-of-plane tearing mode): The crack surfaces slide relatively to each other on their plane and parallel to the crack front, and cause shear stresses ahead of the crack in the direction shown in Figure 2.3 [24].

For Mode I, the remote singular stress fields ahead of a crack tip, which caused by applied remote stress can be calculated using the following set of equation (equations 2.2-2.4) [21]:

$$\sigma_{xx} = \frac{K_I}{\sqrt{2\pi r}} \cos\left(\frac{\theta}{2}\right)\left[1 - \sin\left(\frac{\theta}{2}\right)\sin\left(\frac{3\theta}{2}\right)\right] \qquad 2.2$$

$$\sigma_{yy} = \frac{K_I}{\sqrt{2\pi r}} \cos\left(\frac{\theta}{2}\right)\left[1 + \sin\left(\frac{\theta}{2}\right)\sin\left(\frac{3\theta}{2}\right)\right] \qquad 2.3$$

$$\tau_{xy} = \frac{K_I}{\sqrt{2\pi r}} \cos\left(\frac{\theta}{2}\right) \sin\left(\frac{\theta}{2}\right) \cos\left(\frac{3\theta}{2}\right) \qquad 2.4$$

Also, the crack-tip displacement fields for Mode I can be expressed as follows (equations 2.5-2.6) [21]:

$$u_x = \frac{K_I}{2\mu} \sqrt{\frac{r}{2\pi}} \cos\left(\frac{\theta}{2}\right) \left[\kappa - 1 + 2\sin^2\left(\frac{\theta}{2}\right)\right] \qquad 2.5$$

$$u_y = \frac{K_I}{2\mu} \sqrt{\frac{r}{2\pi}} \sin\left(\frac{\theta}{2}\right) \left[\kappa + 1 - 2\cos^2\left(\frac{\theta}{2}\right)\right] \qquad 2.6$$

where μ is the shear modulus, $\kappa = \frac{3-\nu}{1+\nu}$ (plane stress) and $\kappa = 3 - 4\nu$ (plane strain), where ν is the Poisson's ratio.

2.2.3 Linear elastic fracture mechanics and elastic-plastic fracture mechanics

Fracture mechanics can be classified from different viewpoints. Usually, it is classified into two major categories; linear elastic fracture mechanics (LEFM) and elastic-plastic fracture mechanics [21,22,25]. The LEFM explains fracture processes using linear elasticity theory. Since LEFM is a proper approach especially for fracture in brittle materials, linear fracture mechanics are also identified as brittle fracture mechanics [25]. Brittle fracture applies to materials with linear elastic deformation at the tip of the crack, ideally brittle material (Figure. 2.4 (a)), or with a small amount of plastic deformation, quasi-brittle elastic-plastic material (Figure. 2.4 (b)) [21,25].

In contrast, elastic-plastic fracture mechanics identify fracture processes that are governed by nonlinear material behavior (i.e., plastic deformation) [21,25]. Figure. 2.4 (c) illustrates elastic-plastic fracture mechanics; the crack surfaces moved apart before fracture and created an area with

11

plastic deformation by blunting the tip of the initial sharp crack and led to a finite displacement δ at the tip of the crack [21].

Figure 2.5 shows the loading and unloading paths in both materials, which are identical in the loading paths but different in unloading paths. For nonlinear elastic material, the unloading path follows the loading path. The unloading path of the elastic-plastic material is parallel to the original linear elastic path, with its slope equivalent to Young's modulus [21].
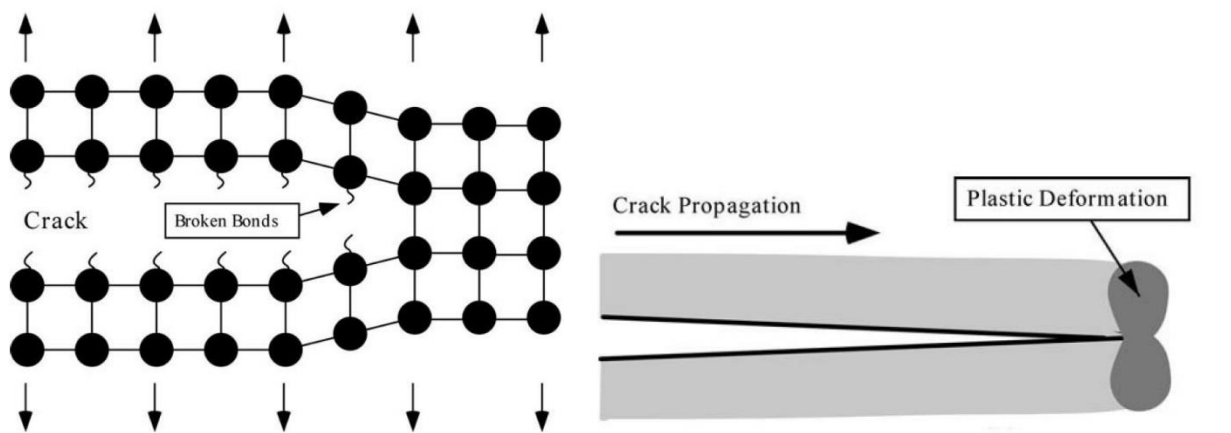
(a) Ideally brittle fracture **(b) Quasi-brittle elastic-plastic fracture**
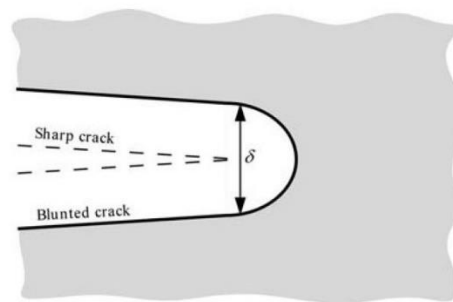
(c) Elastic-plastic fracture

Figure 2.4 The crack propagation in three types of fracture [21]
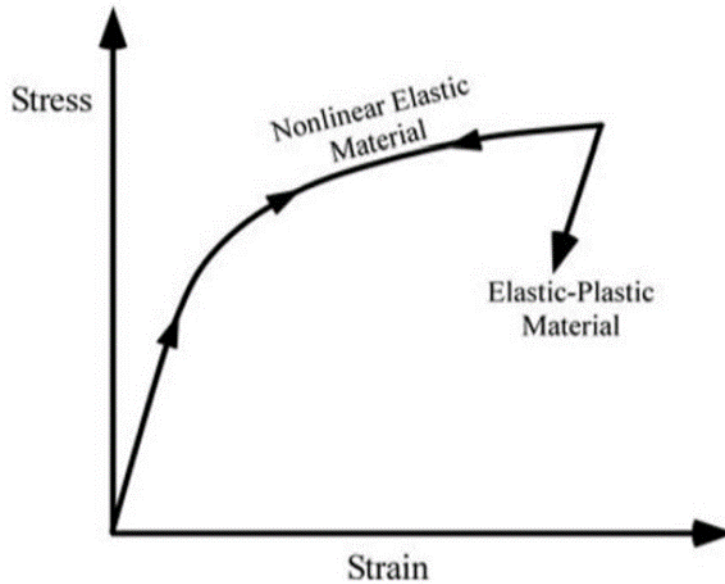
Figure 2.5 The comparision of the nonlinear elastic and elastic-plastic materials under loading and unloading conditions [21].

2.3 Simulation of fracture

2.3.1 Traditional finite element analysis

The finite element method (FEM) is the applicable method in fracture mechanic analysis and capable to approximately predict the stress intensity factor in the absence of exact solutions. FEM has advantages of simplicity and applicability to wide varieties of different loading conditions, materials, as well as geometries [26]. FEM also is applicable to predict fracture response in pipelines. Vazouras et al. [27] investigated the mechanical behavior of buried steel pipelines (grades of X65 and X80) with active strike-slip tectonic fault. They investigated the effects of internal pressure and soil characteristics on the pipelines failure. Hsu [28] analyzed the dynamic elastoplastic modeling of the buried pipelines under seismic ground movement. Their proposed model considered the effect of soil structure to analyze the behavior of soil surrounding the

pipeline. Zhang et al. [29] developed the three-dimensional (3D) FEM for X100 grade of steel pipe with double-ellipsoidal corrosion defect. The effects of the corrosion defect inclination on local stress distribution were investigated. Chen et al. [30] evaluated the mechanical response of damaged steel pipelines with Carbon fiber reinforced polymer using FEM. The effects of maximum acceptable operating pressure and burst pressure on the mechanical response of damaged pipes were investigated and the predicted FEM results were validated with experiments. Although traditional FEMs cannot represent the stress singularity near the crack tip, the method can predict the meaningful values for stress intensity factor for the crack tip using a simple process [26]. FEM is considered an effective method in computational fracture analysis, but three-dimensional mesh generation is burdensome in the simulation of the models with multiple crack formations. Furthermore, modeling the crack topology could be difficult due to considerable refinement needs in the area near the crack tip [31].

2.3.2   Damage based models in finite element analysis

Damage models in material science play a big role in the prediction of rupture under different loading conditions [32]. Different damage models were proposed such as cohesive zone models and continuum damage models to predict failure in complex structures [33]. Cohesive zone model (CMZ) defines the cohesive forces when material elements are separated [34,35]. Parmar et al. [35] used CMZ to investigate the ductile fracture behavior in X70 and X100 grades of pipeline under different constraint conditions. Alvaro et al. [34] used experimental and numerical 3D FEM analysis based on the CMZ to investigate hydrogen embrittlement in the X70 grade of pipeline. Bonora et al. [36] experimentally evaluated damage parameters of the continuum-based damage model in ductile 20MnMoNi55 steel. Their experimental analysis included tension tests on hourglass-shaped samples under multiple and partial unloading to investigate the reliability of

the proposed damage model. Ma et al. [37] proposed a continuum damage model of porous sintered metal under low cycle fatigue loading. Their nonlinear fatigue damage model was used to predict the fatigue damage evolution as well as the cyclic deformation behavior. They also verified their proposed model with experimental and FEM results. Shen et al. [38] numerically and experimental investigated the ductile fracture of a high-strength API X70 pipeline steel. They employed the enHill48 plasticity model in conjunction with Bai–Wierzbicki damage model to accurately predict the anisotropic fracture in this specific grades of steel pipe.

2.3.3 Extended finite element method

To simulate the crack propagating in ABAQUS, XFEM provides a major advantage in comparison with the traditional FEM. In classic FEM, the crack has to follow element edges. On the other hand, in XFEM crack does not need to align with the element edges, which causes XFEM more flexible method [39]. As a result, discontinuities such as crack can be included in the finite element model without any modification of the discretization and the mesh can be built without considering the crack [40]. XFEM is implemented in ABAQUS software and this matter makes it possible for crack to propagate without need of remeshing and matching its geometry. Crack propagation happens when strains and/or stresses surpass a user-defined value (damage criteria) at areas where crack initiates. Damage criteria can be defined as maximum principal strain strain (Maxpe) or stress (Maxps). Maxpe and Maxps along with fracture energy (G_c) as damage evolution criterion are unknown damage parameters, which are being predicted through calibration with experimental results [41].

XFEM can be applied to simulate the initiation and propagation of the crack in pipelines in both small-scale and full-scale tests. For example, in the analysis of the small-scale test, Ameli et al.

15

[42] used Maxps = 1400 MPa for damage initiation and G_c = 200 N/mm for damage evolution in their XFEM analysis to model the Single-Edge Notch Tension (SENT) test of X42 vintage pipelines. Lin et al. [43] obtained Maxps = 750 MPa and G_c = 900 N/mm in XFEM simulation of eight full-scale tests of X52 vintage pipe subjected to complex loading conditions. Okodi et al. [44] predicted burst pressure in the XFEM model of the X70 pipeline using Maxpe and G_c. The validations of XFEM results with tests were applied to investigate the effects of the dent and crack sizes as well as denting pressure on burst pressure [44]. Agbo et al. [45] analyzed the initiation and propagation of X42 vintage pipe using Maxpe and G_c and predicted tensile strain capacity. Also, they investigated the effects of the geometry of the crack and pipe as well as loading conditions on TSC. Okodi et al. [41] in another study simulated the fracture response of X60 grades of the pipeline using Maxpe, and G_c as damage parameters and validated their predicted XFEM results with small-scale and full-scale tests. They also predicted the burst pressure in pipes contained longitudinal cracks using XFEM analysis [41].

Chapter 3: Prediction of tensile strain capacity for X52 steel pipeline materials using the extended finite element method

This chapter was published in Applied Mechanics:

3.1 Abstract

Strain-based design (SBD) plays an important role in pipeline design and assessment of pipelines subjected to geo-hazards. Under such hazards, a pipe can be subjected to substantial plastic strains, leading to tensile failure at locations of girth weld flaws. For SBD, the finite element method (FEM) can be a reliable tool to calculate the tensile strain capacity (TSC) for better design in pipelines. This study aims to investigate the ductile fracture properties for specific vintage pipeline steel (API 5L grade of X52) using the extended finite element method (XFEM). Eight full-scale tests were simulated using the commercial finite element analysis software ABAQUS Version 6.17. Maximum principal strain is used to assess the damage initiation using the cohesive zone model (CZM) when the crack evolution is evaluated by fracture energy release. A proper set of damage parameters for the X52 materials was calibrated based on the ability of the model to reproduce the experimental results. These experimental results included the tensile strain, applied load, endplate rotation, and crack mouth opening displacement (CMOD). This study describes a methodology for validation of the XFEM and the proper damage parameters required to model crack initiation and propagation in X52 grades of pipeline.

3.2 Introduction

With the rapid growth in the pipeline industry, new developments that enable a high operating pressure, long-distance traverses, and a large diameter are essential [4]. Pipeline design, like the majority of structural engineering applications, is a balancing act that aims to maximize the economics and efficiency of a pipeline without sacrificing its safety and reliability. Under the effect of internal pressure, pipeline design is stress-based and acceptable for steel with a well-defined yield ductility, yield point, and strength. However, stress in pipelines can surpass the limit under displacement control loads, such as landslides and earthquakes. In this case, stress-based design can be greatly impractical and inordinately uneconomical [46]. Strain-based design (SBD), on the other hand, is based on displacement-controlled loading and a strain limit state precipitating more practical criteria in designing pipelines subjected to ground movement-induced plastic strains [4,47].

The recent pipeline research literature mostly focuses on modern high-grade pipe materials (X60 and above), while there is little research on vintage lower-grade pipes [3]. Wang et al. [48–50] developed equations to predict the Tensile Strain Capacity (TSC) of pipelines that don't include the effect of internal pressure and are not applicable to vintage pipelines. Similarly, TSC predictive models developed by ExxonMobil (EM) and Pipeline Research Council International (PRCI) are only applicable to modern high-grade pipelines [51–54]. However, a high percentage of vintage pipelines are still in service to transport energy resources, thus it is necessary to develop numerical models that can predict the response of such pipelines under complex loading conditions [5].

The finite-element method (FEM) is a cost-efficient technique in analyzing the pipelines under such loading conditions. The cohesive zone model (CZM) is the applicable numerical tool in FEM used in simulating the propagation of a crack [43]. In CZM, the stress singularity corresponding to linear elastic fracture mechanics at the crack tips is avoided. Complete separation between crack surfaces happens when the cohesive zone stiffness drops to zero [55]. CZM in conjunction with the extended finite element method (XFEM) is widely used in simulating the fracture process [56]. XFEM is an extension to the traditional finite element analysis in which initiation and propagation of cracks that follow arbitrary paths can be simulated without the need for remeshing [5]. Crack or damage initiation in XFEM occurs when a stress or strain based criterion is met while damage evolution follows the CZM model with fracture energy release (G_c) as the input parameter. Ameli et al. [42] used XFEM to obtain the fracture parameters, maximum principal stress (Maxps) = 1400 MPa for damage initiation and G_c = 200 N/mm for damage evolution, by simulating the Single-Edge Notch Tension (SENT) test of X42 vintage pipelines. Similarly, Lin et al. [43] obtained the XFEM set of damage parameters, Maxps = 750 MPa and G_c = 900 N/mm, by simulating the reported eight full scale tests of an X52 vintage pipe subjected to internal pressure, external tensile stress, and bending. However, the use of a stress based damage initiation in XFEM is a bit problematic; both Ameli's and Lin's simulations reported a maximum principal stress that is higher than the ultimate stress of the material, implying that such damage criterion is impractical and probably not applicable to modeling damage in materials subjected to plastifying crack tips.

In the recent literature, XFEM pipeline modeling approaches have started using a strain-based approach as a damage initiation criterion. Liu et al. [57] used XFEM to obtain an appropriate set of damage parameters, namely, maximum principal strain (Maxpe) for damage initiation and fracture energy release (G_c) for damage evolution, to simulate the crack propagation in beam

specimens of X80 pipeline steel. They concluded that Maxpe is a more suitable criterion in comparison with Maxps to simulate the crack propagation. They noticed, however, that the critical strain decreases when the beam specimen thickness increases, suggesting that a fixed criterion might not be suitable for all failure scenarios. Okodi et al. [44] used Maxpe and G_c in XFEM analysis to predict burst pressure in X70 pipe specimens with the cent-crack defect. They investigated the effects of denting pressure as well as dent and crack sizes on burst pressure and validated the predicted XFEM results with experiments [44]. Okodi et al. [41] simulated the propagation of cracks in X60 grades of the pipeline using XFEM damage criterion, Maxpe, and G_c, and validated their results with small-scale and full-scale tests. They used proposed XFEM models to predict the burst pressure in pipes with external longitudinal rectangular cracks [41]. Agbo et al. [45] predicted the ductile fracture response of an X42 vintage pipe under biaxial loading using Maxpe and G_c and obtained the TSC of this specific grade of pipes. The effects of loading conditions, as well as the geometry of the crack and pipe on TSC, were also investigated in this research. Agbo et al. [5] calculated the strain-based XFEM damage parameters, Maxpe = 0.013 and G_c = 450 N/mm, and TSC for an X42 vintage pipeline through calibrating numerical results with full-scale test results.

In the present study, a strain-based fracture criterion is used to simulate fracture initiation in full-scale tests of pressurized pipes, and a set of parameters to provide the TSC of X52 steel pipeline material is found. Maxpe is chosen as the damage criterion. In contrast to Maxps, which was used previously by Lin et al. [43] to predict the fracture response of this grade of vintage pipeline, Maxpe critical values are relatable to the physical critical strain values expected in the vicinity of the crack tip [5]. The crack initiation and propagation are numerically predicted through simulating eight published full-scale tests of X52 vintage pipes that are subjected to the combination of

internal pressure and external eccentric tension which were reported by Abdulhameed et al. [58].

A proper set of damage parameters for X52 grades of pipes is obtained by calibrating the XFEM

model implemented in ABAQUS [59]. The numerical results are compared with data from eight

full-scale experimental tests including tensile strain and CMOD at failure, applied force, and

rotation at end plates.

3.3 Full-scale test experiment

The fracture behavior of vintage API 5L grade X52 steel pipes was investigated experimentally by

Abdulhameed et al. [58] and Lin [16]. The experimental work included full-scale and small-scale

tests. For the full-scale test, eight pipe specimens were cut out of the vintage X52 pipeline grade

with girth welds situated in the middle length of each sample. The pipe specimens had a wall

thickness of 6.9 mm and an outer diameter of 324 mm. A circumferential crack-like defect was

created in each pipe sample on the outer surface of the pipe close to the girth weld. The

circumferential flaw length was 5% or 15% of the pipe circumference, while the flaw depth was

25% or 50% of the pipe wall thickness [58]. For small-scale tests, 25 tension coupon tests were

used to obtain the tensile properties of the X52 grade of pipeline. The specimens were machined

from different locations of the X52 pipe sample; 13 small round specimens were machined from

the circumferential direction, and 12 standard rectangular specimens were machined from the

pipe's longitudinal direction [16]. Also, 24 Charpy V-notch (CVN) impact tests were performed

by Lin [16] to obtain the fracture properties of X52 vintage pipeline specimens.

3.4 Problem formulation and the XFEM model

In this study, the strain-based damage parameters Maxpe and G_c were obtained for the X52 pipe

XFEM model. Eight 3D XFEM models were developed in ABAQUS software to simulate the

21

experiments. Table 3.1 presents the dimensions of the full-scale tests and initial cracks as well as the applied internal pressure. Figures 3.1 and 3.2 show the schematic and the finite element (FE) configuration of the model, respectively. In order to reduce the analysis time and the computational effort, the center part of the pipe was modeled as a solid part (40 mm long), while the side parts were modeled as shells, as shown in Figure 3.1. A shell–solid coupling constraint was used at the junction between the shell and solid parts. Additionally, only half of the pipe on the longitudinal side was modeled to take advantage of the symmetry of the pipe around the YZ plane (Figure 3.1). The pipe model contains two endplates and two loading tongues; both are modeled as shell planar rigid bodies represented by reference nodes with 50 mm eccentricity from the pipe's longitudinal axis. The tie constraint was used to connect the endplates to the shell parts to simulate the perfectly welded joints. Lastly, a tie constraint connecting the loading tongues to the endplates at an eccentricity of 50 mm was used to model the experimentally applied eccentric loading. The XFEM circumferential crack was modeled as a shell planar part and located in the middle length of the solid part (Figures 3.1 and 3.2). Shell parts, tongues, and endplates were meshed using four-node linear shell element with reduced integration and hour-glass control (S4R).

Table 3.1 Basic information of tests and models

Test /Model	Pipe specimen dimensions			Crack dimensions		Internal pressure level	
	Outer diameter (mm)	Pipe length (mm)	Wall thickness (mm)	Crack depth (mm)	Crack length (mm)	Internal pressure (MPa)	Hoop stress/SMYS (%)
Test 1	324	1828.8	6.95	1.7	50	11.65	75
Model 1	324	1828.8	6.8	1.7	50	11.65	77
Test 2	324	1828.8	6.8	1.5	50	3.50	23
Model 2	324	1828.8	6.8	1.5	50	3.50	23

Test 3	324	1828.8	6.8	3.1	50	11.67	77
Model 3	324	1828.8	6.8	3.1	50	11.65	77
Test 4	324	1828.8	6.8	3.3	50	4.70	31
Model 4	324	1828.8	6.8	3.3	50	4.65	31
Test 5	324	1219.2	6.8	1.4	150	11.65	77
Model 5	324	1219.2	6.8	1.4	150	11.65	77
Test 6	324	1219.2	6.8	1.8	150	4.60	31
Model 6	324	1219.2	6.8	1.8	150	4.65	31
Test 7	324	1219.2	6.8	3.5	150	11.65	77
Model 7	324	1219.2	6.8	3.3	150	11.65	77
Test 8	324	1219.2	6.8	2.7	150	4.65	31
Model 8	324	1219.2	6.8	2.7	150	4.65	31

The global mesh size was 5 mm for the shell parts and 10 mm for tongues and endplates. The solid part was meshed with an 8-node linear brick element with reduced integration and hourglass control (C3D8R) as well.
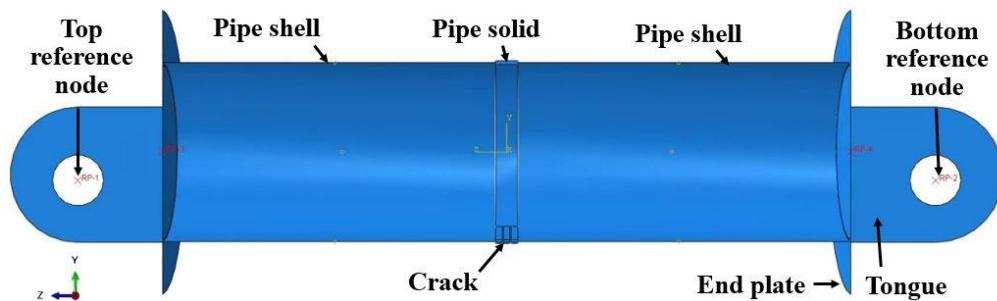
Figure 3.1 Assembled components of pipeline XFEM model showing the geometry and reference points.

Based on mesh convergence analysis performed by Lin et al. [43], a finer mesh (0.5 mm) was used in the partitioned zone near the crack propagation path and a coarser mesh (5 mm) was used in the area far from the crack to guarantee the accuracy of calculation as displayed in Figure 3.2. The

mesh construction in the solid part was generated with a mesh size between 0.5 and 5 mm. The finer mesh, including elements with a height of 0.5 mm, a thickness of 2 mm, and a length of 0.5 mm, was applied in the partitioned region near the crack propagation line. The element height was in the direction of the crack propagation line, and element thickness and length were parallel and perpendicular to the crack plane, respectively.

The pipe was simulated using the elasto-plastic isotropic hardening material model. The yield stress and plastic strain parameters were taken from the average of true stress–strain curves obtained from the small-scale tension test carried out on X52 pipe specimens by Lin [16]. The true stress-strain curve is shown in Figure 3.3 and the parameters used as material properties in the XFEM models are shown in Table 3.2. Maxpe and G_c were selected as two damage criteria to predict the initiation and propagation of the crack in the XFEM model of the X52 vintage pipe, respectively. Failure in the model was defined as the onset of the crack tip (or element damage) reaching the inner edge of the last element of the wall thickness. Since the experimental results from Abdulhameed et al. [58] showed that failure in the X52 occurred in the base metal, the material properties of the base metal were applied for the whole pipe. To compare the predicted XFEM results with experimental results, the ratios of test-to-model predictions and the concomitant coefficient of variation (COV) of the ratios were calculated in the current study, in which COV = the standard deviation/the mean of the ratios of test-to-model predictions of all eight tests.
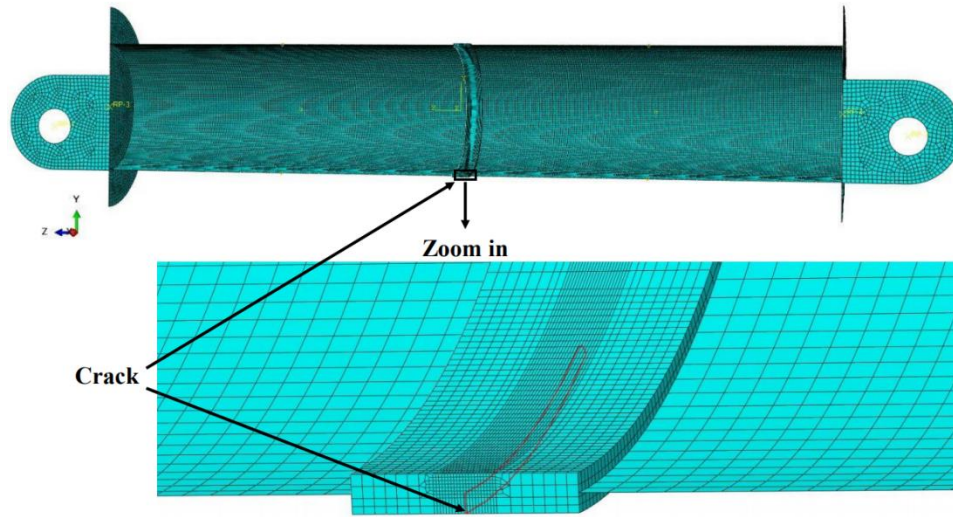
Figure 3.2 Mesh pattern of the XFEM model of pipeline and location of a circumferential crack.
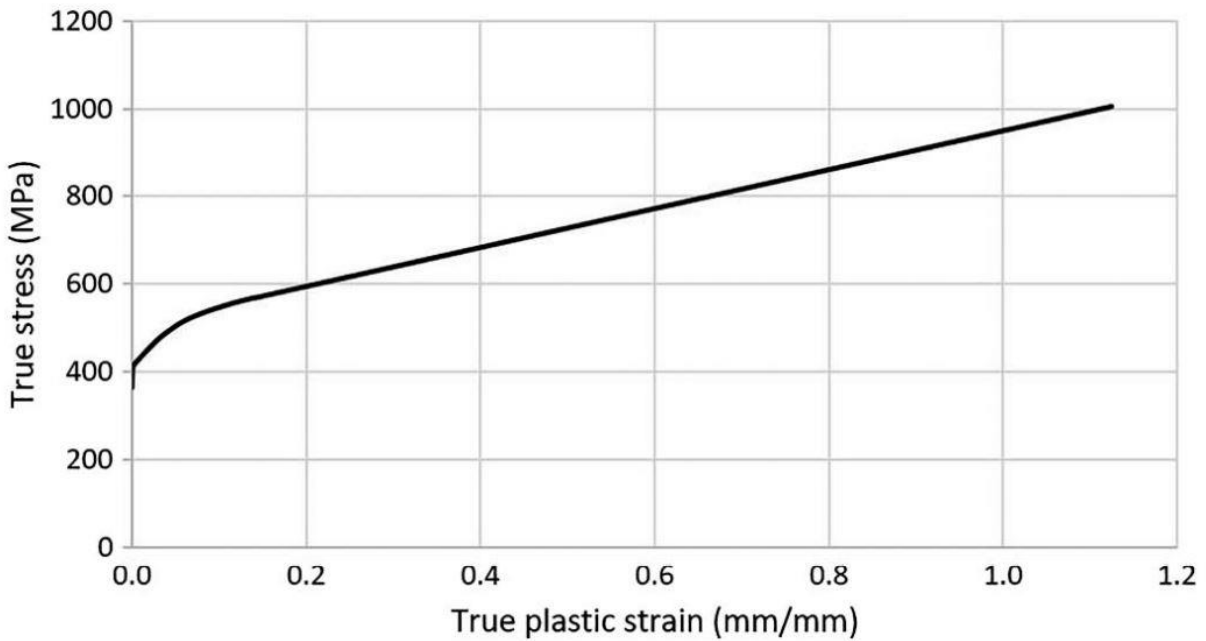
Figure 3.3 Average true stress-plastic strain curve of the X52 pipe material.

Table 3.2 Material properties of the X52 pipe [16].

Young's modulus (GPa)	Poisson's ratio	0.2% Offset yield strength (MPa)	Ultimate true plastic strain
199	0.3	411	0.147

3.5 Results and discussion

3.5.1 Tensile strain capacity comparison with experiments

Two sets of damage parameters are used in the analysis. The first set is obtained through calibration in two steps. First, the damage sets which can accurately predict each of the eight experiments are obtained independently for every model. Then, by obtaining the proper range of Maxpe and G_c for all models, the final set of parameters that can predict all eight models with minimum calibration errors are obtained. The final damage parameters (Maxpe = 0.085 mm/mm and G_c =900 N/mm) are proposed as fracture properties of X52 vintage pipe. The second set of damage parameters (Maxpe= 0.013 mm/mm and G_c =450 N/mm) were previously obtained by Agbo et al. [5] in the simulation of the ductile X42 grade of pipeline and applied in the current analysis for comparison.

Figures 3.4 and 3.5 represent the XFEM longitudinal tensile strain distribution at the onset of failure and its comparison with longitudinal tensile strains obtained from tests. For each model, the tensile strain values were calculated on the pipe's outer surface and plotted throughout the pipe length at the tension side. As it can be observed in Figures 3.4 and 3.5, generally, a good agreement is obtained between the experiments and the XFEM results. Apart from models 5 and 6, it is seen in these two figures that the damage parameters selected in the XFEM model (Maxpe = 0.085 and G_c = 900 N/mm) are appropriate for the modeled X52 grade. It must be emphasized that the tensile strain capacity is defined as an "average" value of the strain around the flaw since the strain profile is disrupted at the flaw location [58]. The simulation cannot accurately predict the tensile strain results with a distance less than 20 mm from the crack tip due to the complex stress-strain state near the crack tip. Similar to the observed experimental distribution, the tensile strain increases from the crack location at the pipe centre towards the pipe ends.

The TSC is calculated from the XFEM tensile strain values in Figures 3.4 and 3.5 and compared with those obtained from full-scale experiments and presented in Figure 3.6 and Table 3.3. In this study, the TSC was defined as the average tensile strain at failure. The TSC is obtained by averaging tensile strain values from 10% to 40% of the pipe length on both sides far from the crack, which is in the range of 185–730 mm for tests and models 1–4, and 120–490 mm for tests and models 5–8. Table 3 represents the mean of the ratios (test/model) and COV (%) between XFEM and test results. Additionally, Figure 6 shows the comparisons between two results with a 45-degree line. The comparisons show that XFEM TSC values underestimate the test results. Comparing the results of Figures 3.4 and 3.5 with the CMOD-applied load (Figures 3.8 and 3.9) and rotation-applied load results (Figures 3.11 and 3.12) indicates that using Maxpe of 0.085 and G_c of 900 N/mm slightly underestimates the TSC results, but in CMOD-applied load and rotation-applied load results, higher prediction can be observed in some models in comparison with the test results.

Choosing higher Maxpe values (Maxpe = 0.11 and G_c = 900 N/mm) results in TSC values that better match the experimental results with less variability and percentage differences, as presented in Table 3.3, but sacrifices the accuracy in the results of CMOD-force (Figures 3.8 and 3.9) and rotation-force (Figures 3.11 and 3.12). Therefore, the set of Maxpe of 0.085 and G_c of 900 N/mm is chosen to balance the accuracy in all three types of numerical results. Additionally, the percentage differences in Table 3.3 and Figure 3.6 are a bit misleading since the distributions shown in the Figures 3.4 and 3.5 show a good agreement between the numerical and experimental results and indicate the capability of the XFEM model to predict the TSC of X52 vintage pipes.
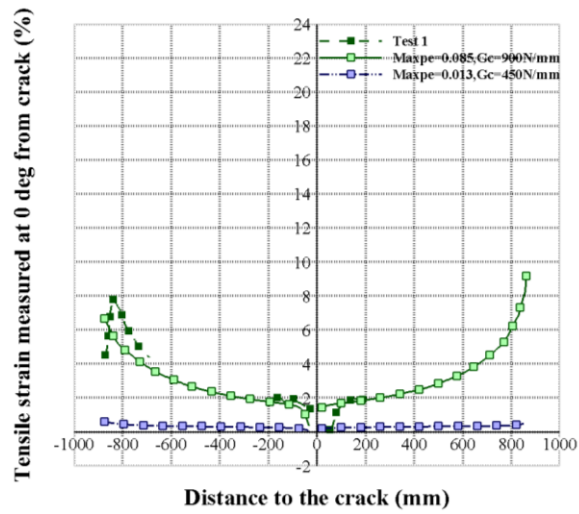
(a)
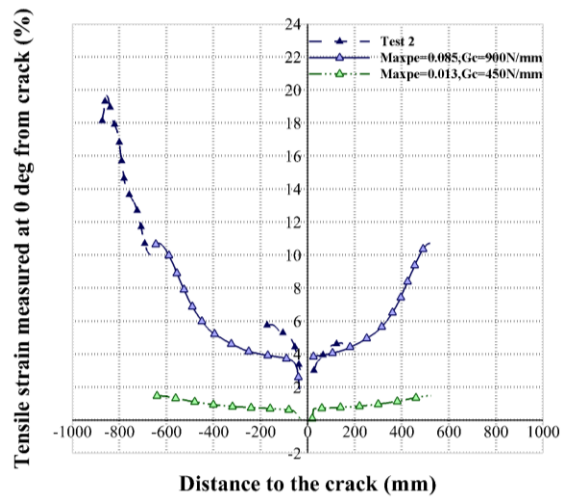
(b)
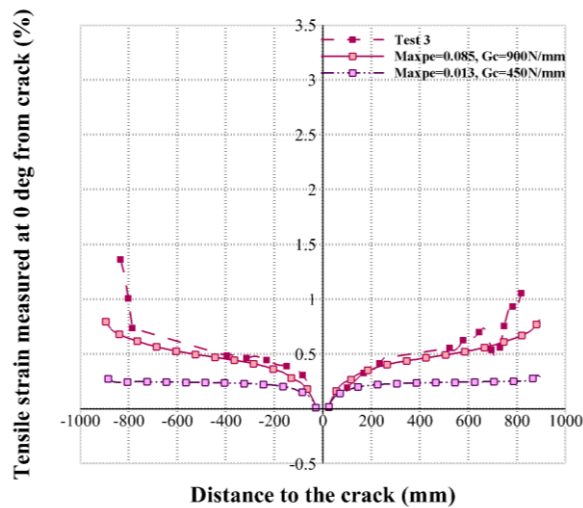
(c)
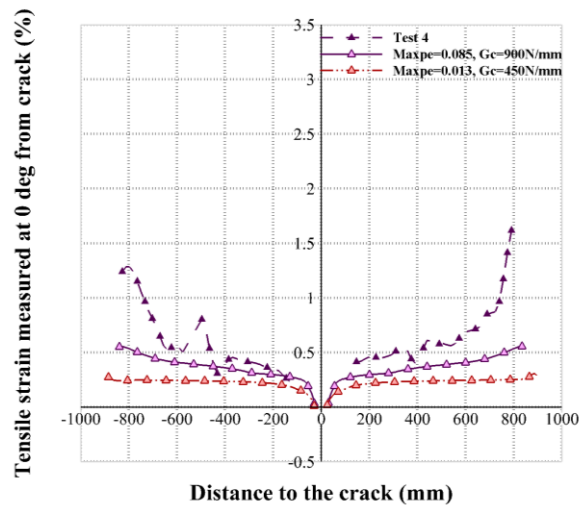
(d)

 Figure 3.4 Comparison of tensile strains measured along the pipe length at failure obtained from models and tests 1-4 (a-d, respectively).
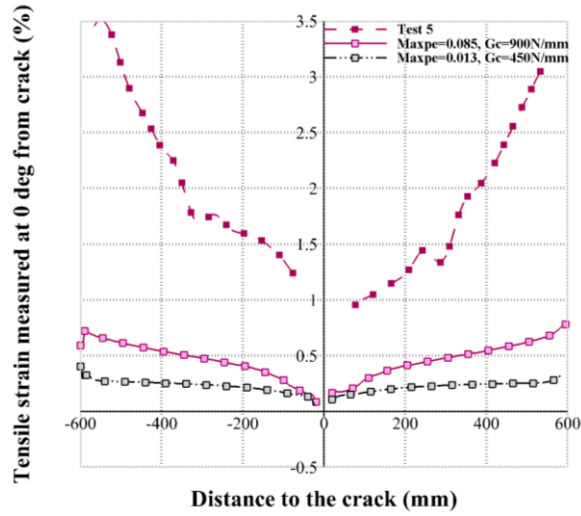
(a)
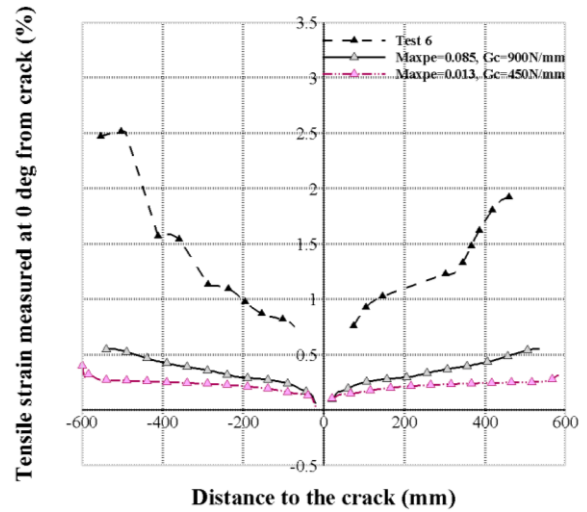
(b)
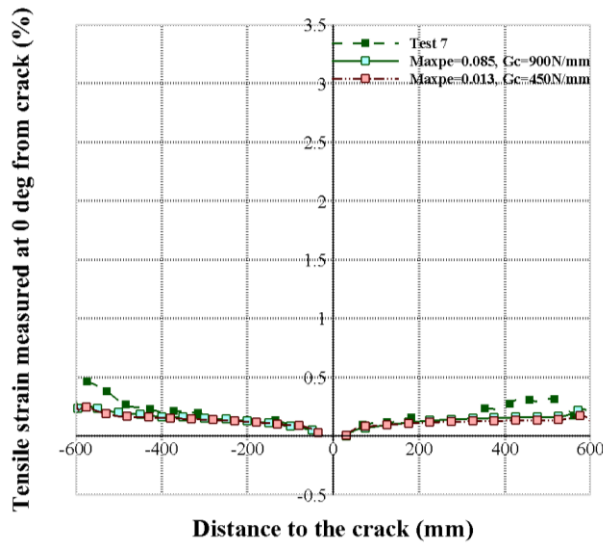
(c)
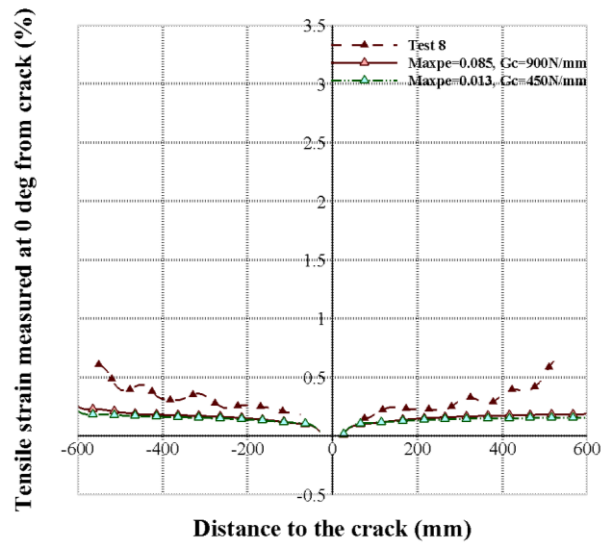
(d)

Figure 3.5 Comparison of tensile strains measured along the pipe length at failure obtained from models and tests 5-8 (a-d, respectively).

Models 5 and 6 showed the biggest difference in TSC values between numerical and test results, as shown in Figures 3.5 (a) and (b) and percentage difference in TSCs in Table 3.3. One explanation could be the higher material properties of the pipes used in tests 5 and 6 in comparison

with other pipes or the different thickness at the location of the flaw, which increases the fracture resistance of the pipe, leading to higher strains.

Table 3.3 TSCs of XFEM models and full-scale tests.

Model/Test	Test TSC (%)	XFEM TSC Maxpe = 0.085 G_c = 900N/mm (%)	Difference (%)	Ratio (Test/Model)	XFEM TSC Maxpe = 0.11 G_c = 900N/mm (%)	Difference (%)	Ratio (Test/Model)
1	4.187	2.730	34.798	1.534	3.0680	26.726	1.365
2	11.25	6.310	43.911	1.783	7.0750	37.100	1.590
3	0.537	0.476	11.359	1.128	0.600	−11.732	0.895
4	0.546	0.372	31.868	1.468	0.415	23.992	1.316
5	1.829	0.478	73.865	3.826	0.628	65.660	2.912
6	0.726	0.373	48.622	1.946	0.432	40.495	1.681
7	0.217	0.146	32.719	1.486	0.151	30.414	1.437
8	0.312	0.165	47.115	1.890	0.170	45.510	1.835
Mean (Ratios)	-	-	-	1.883	-		1.629
COV (%)	-	-	-	44.038	-		36.228

Another possibility could be the higher percentage of multiple notches in the machined flaw observed in the metallurgical study of test 5 in comparison with other tests leading to higher fracture energy and, eventually, higher strain [58]. Calibration of damage parameters in the XFEM for models 5 and 6 showed that when Maxpe = 0.2 and G_c = 900 N/mm, the XFEM results are in good agreement with the tests (Figure 3.7).

3.5.2 CMOD, applied tension force, and end plate rotation

The CMOD-applied load curves were obtained numerically using the damage parameter Maxpe = 0.085 and G_c = 900 N/mm and compared with the experimental results and are presented in

Figures 3.8 and 3.9 as well as in Table 3.4. As it can be observed from Figures 3.8 and 3.9, all the obtained curves show the same nonlinearity pattern, similar to that observed in the tests, starting with zero initial slopes with a precipitous rise near failure.

(a)   **(b)**
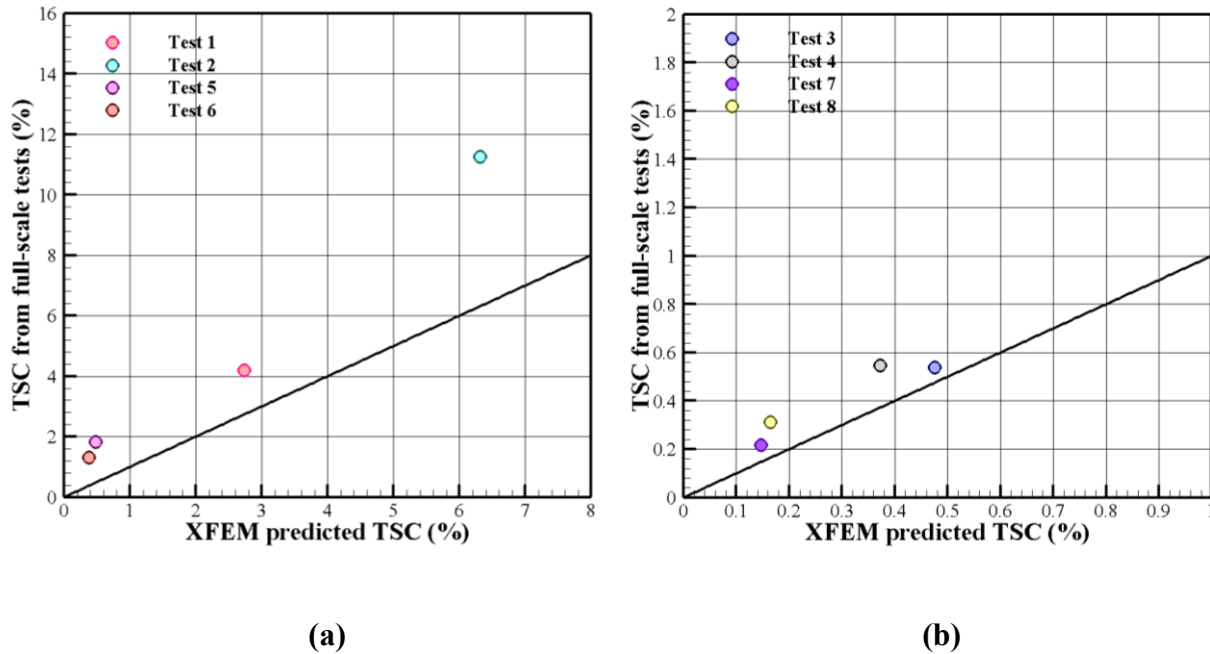
Figure 3.6 Comparison of TSCs obtained from XFEM models and experiments 1-4 (a), and 5-8 (b).

$CMOD_{critical}$ which was proposed by Abdulhameed et al. [58], and calculated at the point where CMOD rapidly increases and the applied load is almost constant. $CMOD_{critical}$ equals CMOD at 97% of the failure load. In Table 3.4, the $CMOD_{critical}$ values for all tests and models are compared with the results of $CMOD_{failure}$, which is the CMOD value when the failure occurs, as described previously and shown in Figure 3.10. The numerical $CMOD_{failure}$ values were between 33% lower to 12% higher than the experimental $CMOD_{failure}$. The maximum difference equals to 0.74 mm was obtained in Test and Model 3. The endplate rotations obtained from the XFEM are also plotted against the applied load and compared with experiments. The results are shown and summarized

31

in Figures 3.11and 3.12 and Table 3.4, respectively. A good agreement is observed for all the models and tests.

(a)

(b)

(c)
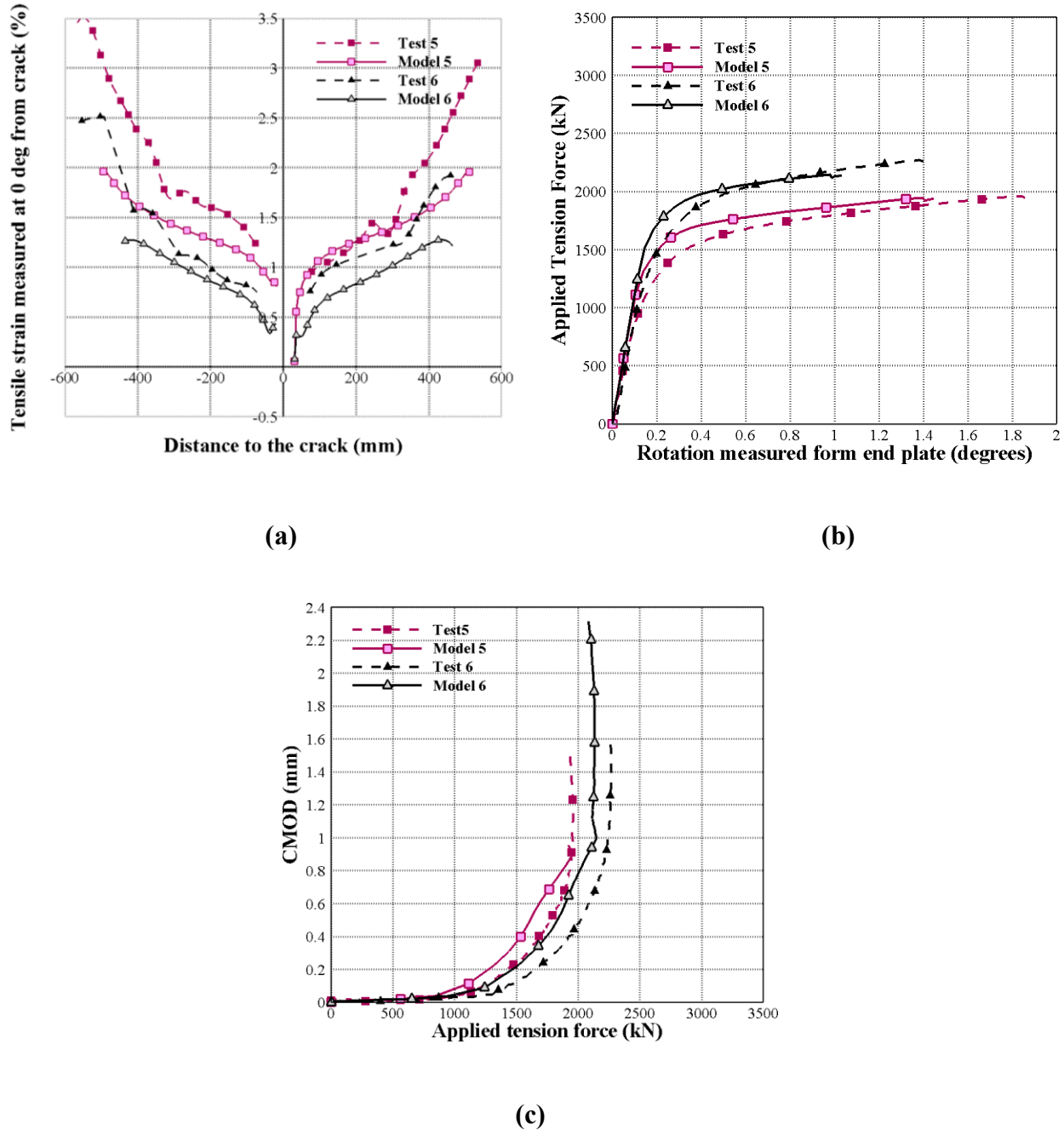
Figure 3.7 Comparison of (a) tensile strains measured along the pipe length at failure, (b) rotation–force curves, and (c) force–CMOD curves obtained from models and tests 5 and 6 (Maxpe = 0.2 and G_c = 900 N/mm).
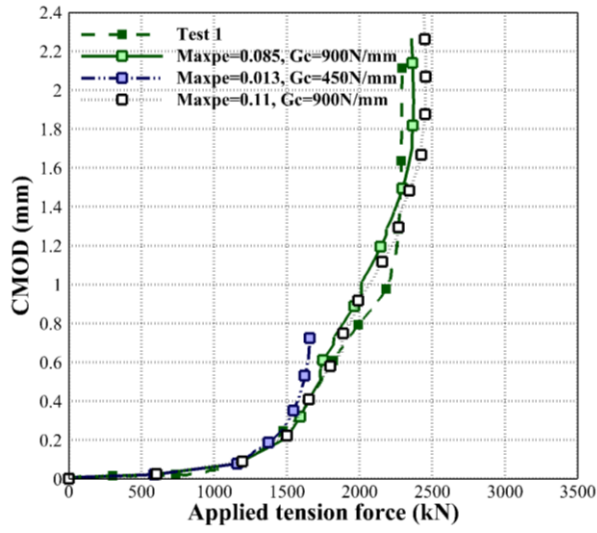
(a)
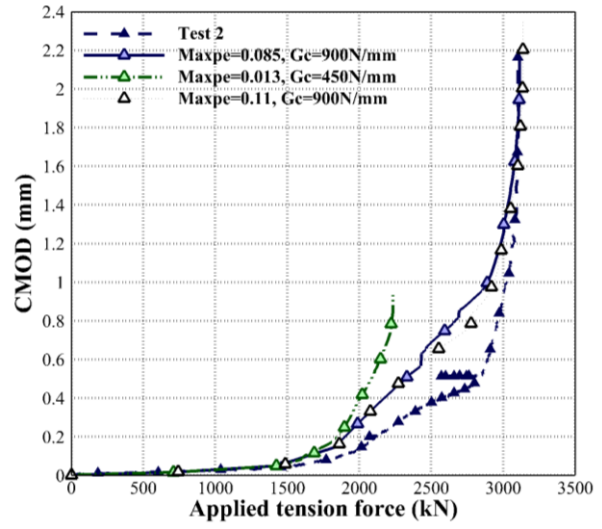
(b)
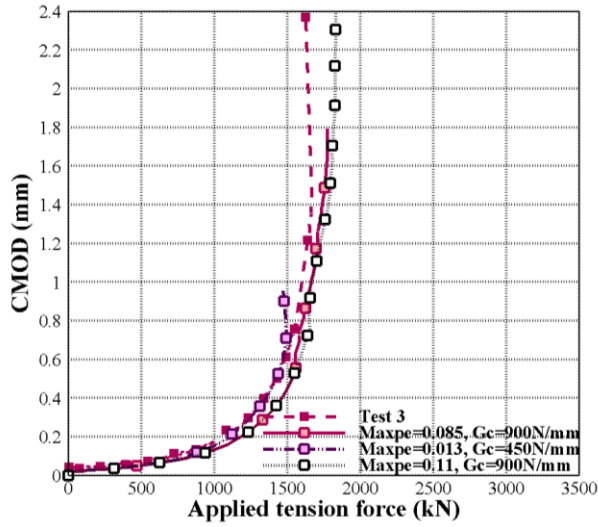
(c)
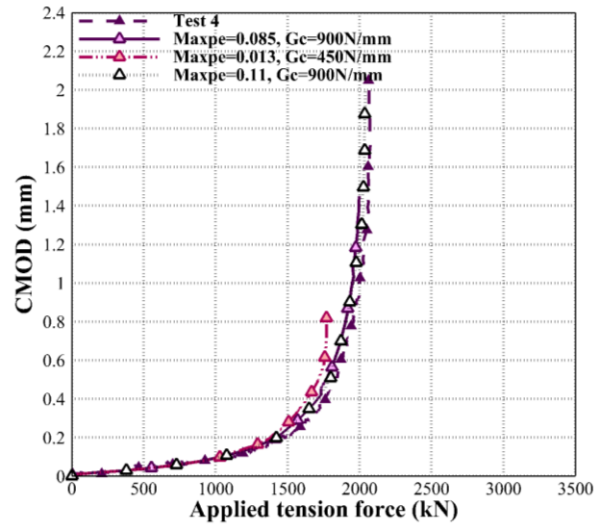
(d)

Figure 3.8 Comparison of force-CMOD curves obtained from models and tests 1-4 (a-d, respectively).

33
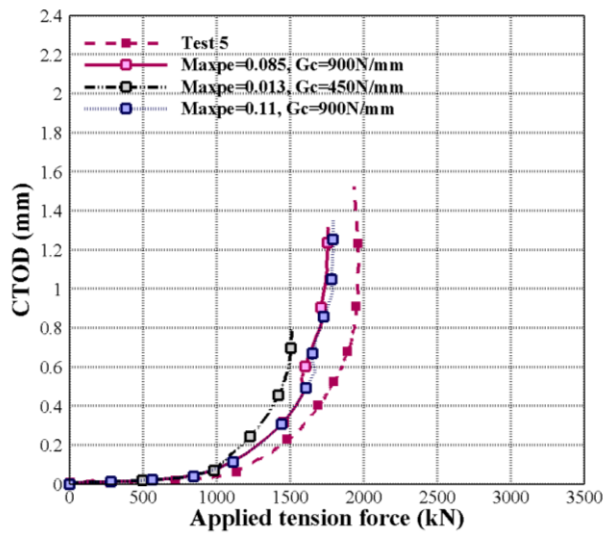
(a)
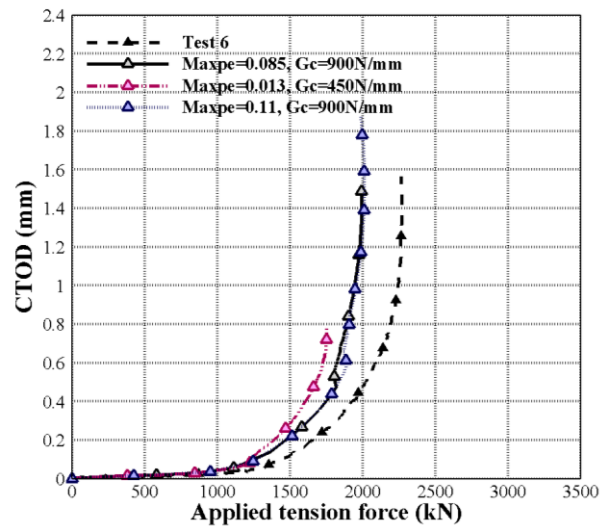
(b)
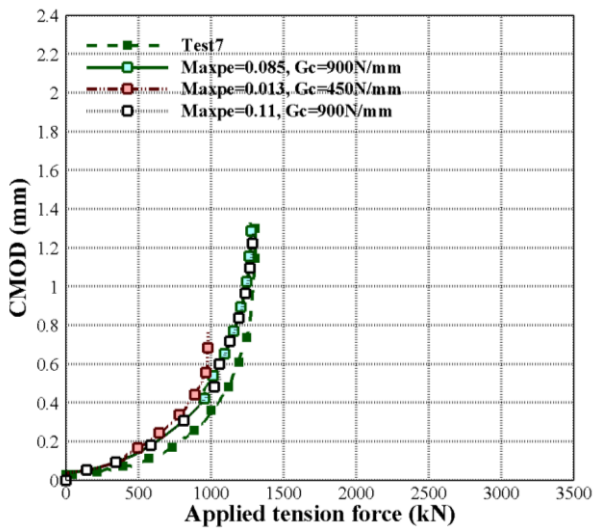
(c)
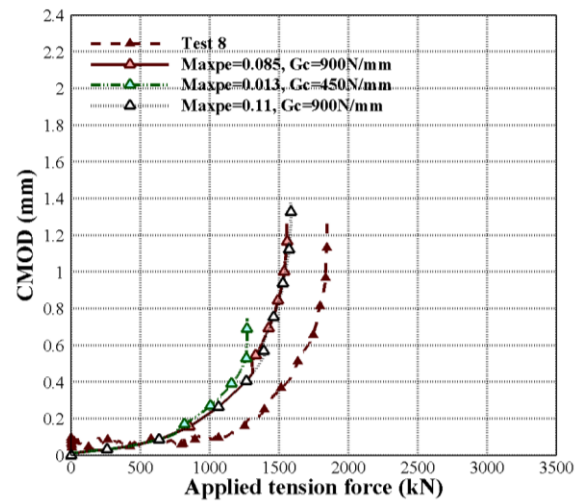
(d)

Figure 3.9 Comparison of force-CMOD curves obtained from models and tests 5-8 (a-d, respectively).

Table 3.4 Comparison between XFEM results and tests at failure.

Model/Test	Max Load (kN)	Rotation at Endplate (Degrees)	CMOD$_{failure}$ (mm)	CMOD$_{critical}$ (mm)	Reduction in Pipe Wall Thickness (%)
Test 1	2299	5.080	2.110	1.190	32.400
Model 1	2360	5.135	1.910	1.508	16.050
Difference (%)	2.661	1.093	−9.455	26.723	−50.462
Ratio	0.974	0.989	1.105	0.789	2.019
Test 2	3100	6.820	2.160	1.090	27.900
Model 2	3112	5.634	2.060	1.367	14.253
Difference (%)	0.415	−17.391	−4.611	25.413	−48.914
Ratio	0.996	1.211	1.049	0.797	1.957
Test 3	1623	0.980	2.370	1.180	19.100
Model 3	1773	0.847	1.631	1.304	10.032
Difference (%)	9.259	−13.578	−31.169	10.508	−47.476
Ratio	0.9153	1.157	1.453	0.905	1.904
Test 4	2061	1.040	2.050	1.160	20.600
Model 4	1996	0.663	1.373	0.943	8.107
Difference (%)	−3.145	−36.242	−33.035	−18.707	−60.64
Ratio	1.032	1.569	1.493	1.230	2.541
Test 5	1934	1.860	1.520	0.770	26.500
Model 5	1755	0.621	1.693	0.761	16.850
Difference (%)	−9.218	−66.588	11.395	−1.169	−36.415
Ratio	1.102	2.995	0.898	1.0119	1.572
Test 6	2261	1.400	1.560	0.900	27.900
Model 6	1990	0.506	1.745	0.878	15.325
Difference (%)	−11.981	−63.820	11.829	−2.444	−45.072
Ratio	1.136	2.767	0.894	1.025	1.821
Test 7	1304	0.260	1.300	0.900	19.100
Model 7	1275	0.204	1.273	0.998	8.295
Difference (%)	−2.254	−21.664	−2.061	10.888	−56.571
Ratio	1.023	1.275	1.021	0.902	2.303
Test 8	1831	0.420	1.270	0.850	20.600
Model 8	1556	0.221	1.152	0.898	7.295
Difference (%)	−15.018	−47.314	−9.274	5.647	−63.146
Ratio	1.177	1.900	1.102	0.947	2.824
Mean (Ratios)	1.044	1.733	1.127	0.951	2.118
COV (%)	8.390	44.086	20.281	14.950	19.377

As shown in Table 3.4, the XFEM results for maximum loads are approximately between 15% lower and 9% higher than the experiments for all tests and models. The maximum difference of 275 kN was obtained between test and model 8. Additionally, it can be seen that the XFEM rotations at failure are roughly from 67% lower to 1% higher than the experiments for all tests and models, with a maximum difference of 1.2 degrees calculated between test and model 5.
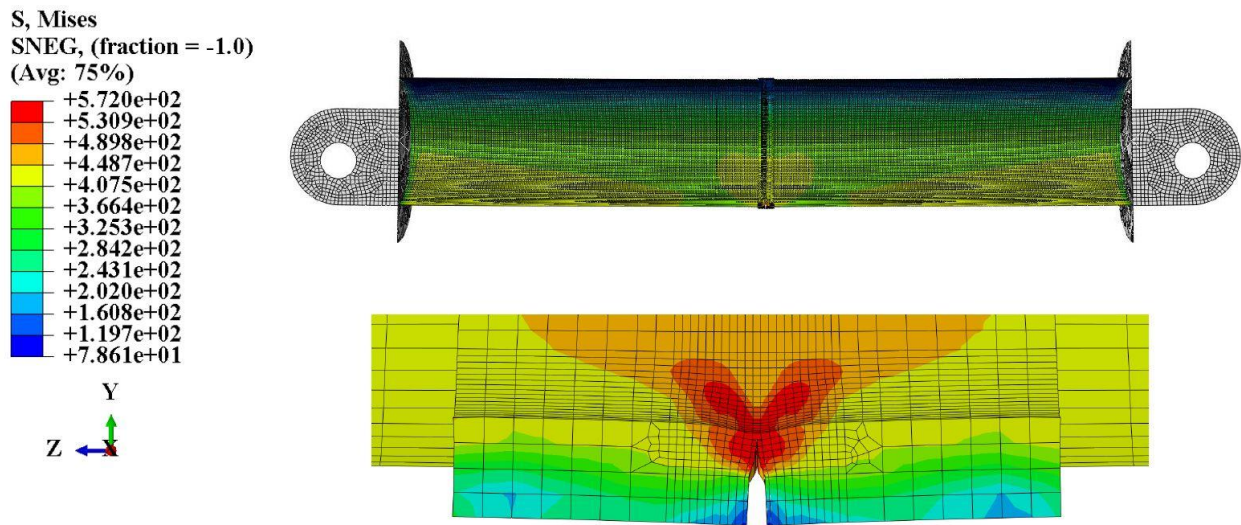
Figure 3.10 The CMOD$_{failure}$ for the model 4.

It is concluded that in tests 5 and 6, using Maxpe of 0.085 and G_c of 900 N/mm produce the biggest difference in results, as shown in Figures 3.9(a) and (b) for CMOD-force and Figures 3.12(a) and (b) for rotation-force results. The experimental observations showed higher fracture resistance than the models, as discussed previously. When a Maxpe of 0.2 is chosen for these tests, better predictions can be observed (Figures 3.7(b) and (c)). Future work will attempt to obtain the material damage parameters from small-scale tests and to develop a variable failure criterion that is a function of the crack tip constraints.

The damage parameters (Maxpe = 0.013 and G_c = 450N/mm) obtained by Agbo et al. [5] for X42 vintage material were used as damage parameters in this study to test whether these parameters can universally be used among different vintage pipelines or not. The results show underestimation of the TSC (Figures 3.4 and 3.5), CMOD-applied load (Figures 3. 8 and 3.9), and rotation-applied load (Figures 3.11and 3.12) for all eight models in comparison with test results, which shows that Maxpe = 0.013 and G_c = 450 N/mm are not a proper damage set for X52 vintage pipe. This poor prediction could be attributed to the difference in the location of the cracks

36

in both sets. For Agbo et al.'s tests, the flaws were machined in the reportedly inferior weld material, in contrast with the X52 where failure occurred in the base metal [5,58].

(a)

(b)

(c)

(d)
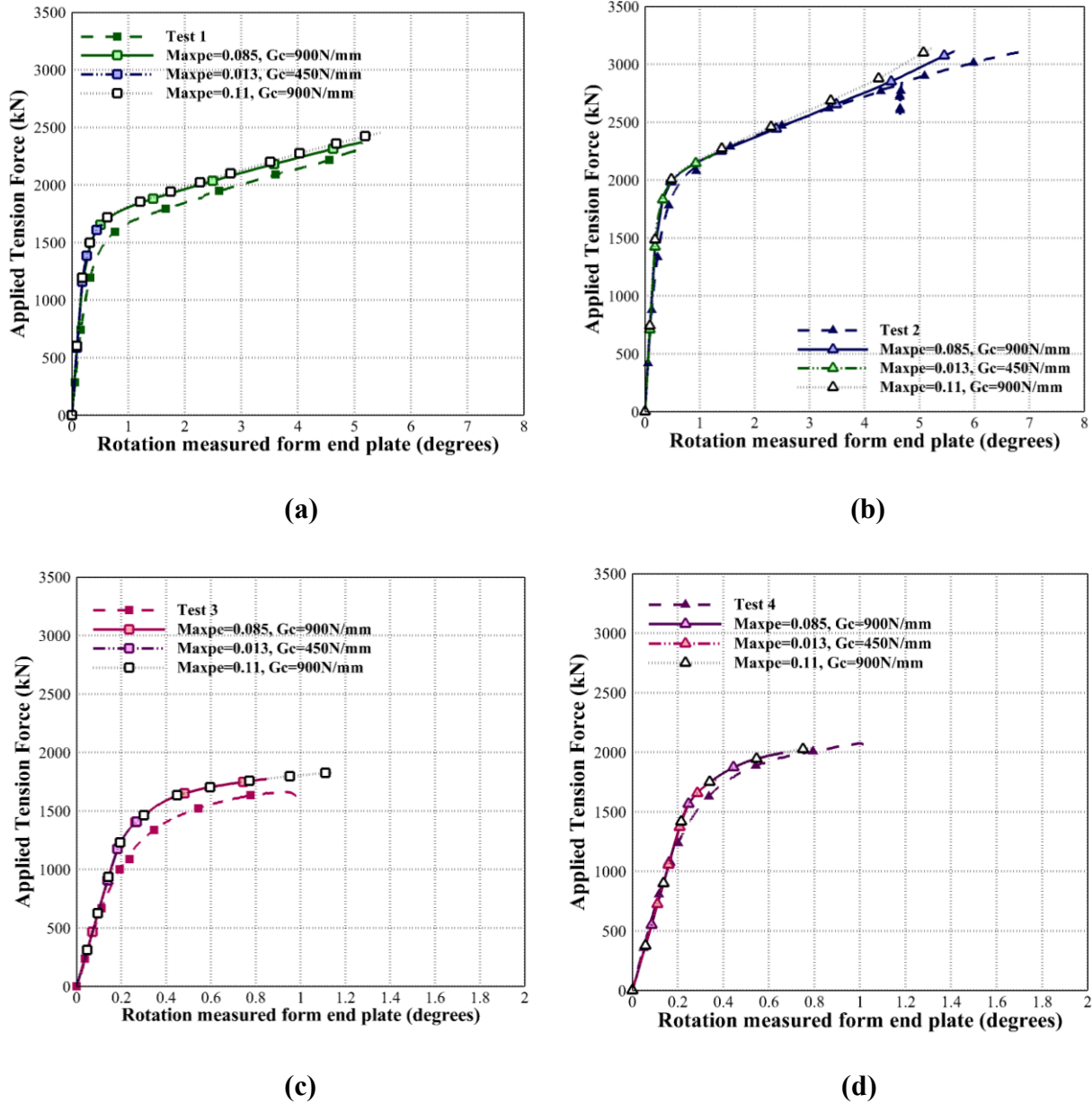
Figure 3.11 Comparison of rotation-force curves obtained from models and tests 1-4 (a-d, respectively).

There is a need for a larger set of experimental results to correlate the material damage parameters with the quality of the weld metal and the grade and toughness of the base metal.
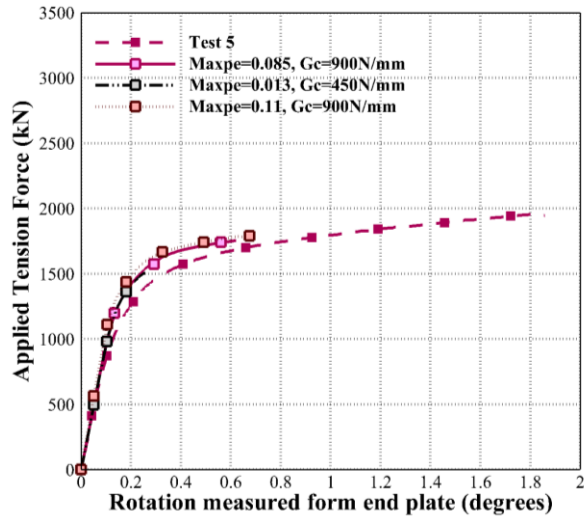
(a)
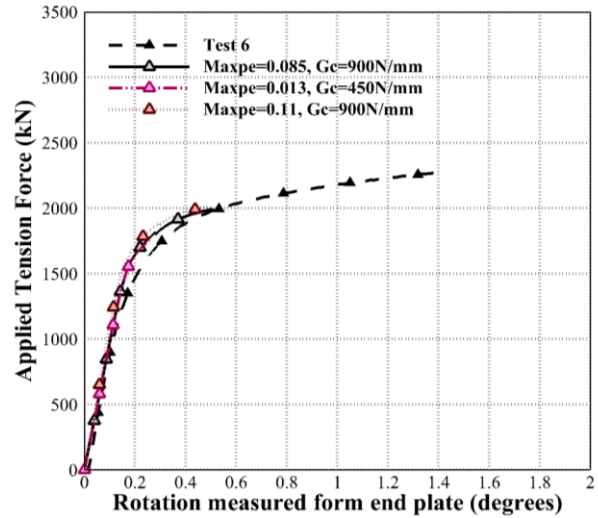
(b)
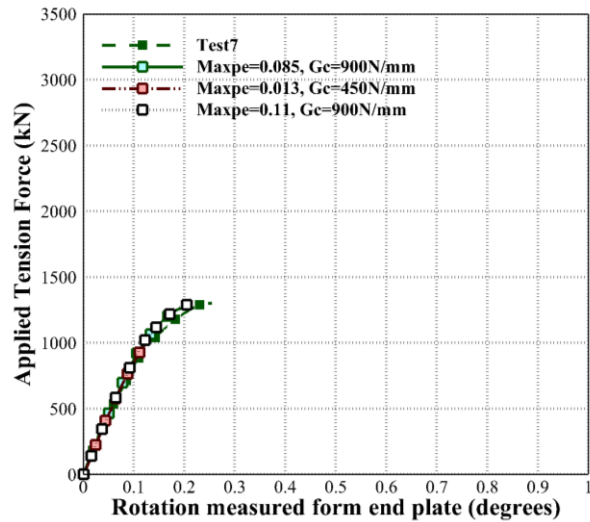
(c)
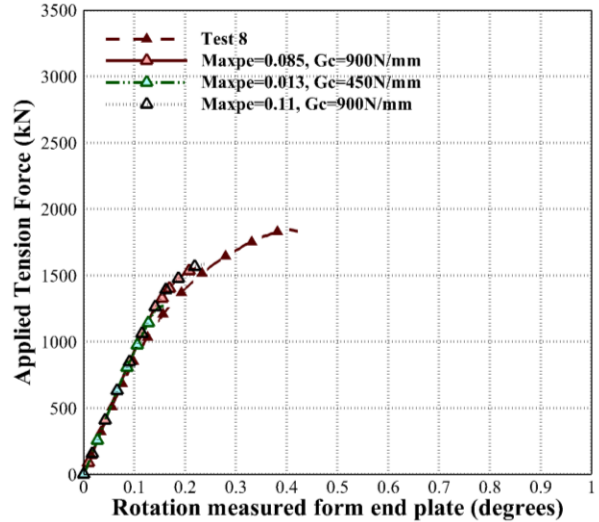
(d)

Figure 3.12 Comparison of rotation-force curves obtained from models and tests 5-8 (a-d, respectively).

3.5.3 Geometry of cracked pipe in the vicinity of the flaw

The numerical fracture surface analysis at failure for X52 pipe was performed by Lin et al. [43] using the XFEM and damage parameters Maxps = 750 MPa and G_c = 900 N/mm. The fracture

38

surface compared well with experiments presented by Abdulhameed et al. [58]. Figure 3.13 shows the fracture surface of model 1 when Maxpe = 0.085 and G_c = 900N/mm and the fracture geometry obtained by fractography of test 1. The parameters A, C, and E represent original pipe wall thickness, reduced pipe wall thickness, and original crack depth, respectively. The experimental analysis of fracture surfaces revealed that fracture surfaces were flat with no significant ductile dimpling or tearing, suggesting a fracture that is brittle in nature [58]. A comparison of the reduction in wall thickness at failure with the experimentally observed value is presented in Table. 3.4. The results show that the model consistently underestimates the reduction in the wall thickness at the onset of failure (mean = 2.118 and COV = 19.377%). One reason for this discrepancy as proposed by Lin et al. [43] is the exclusion in the numerical analysis of the mechanical deformation associated with the sudden release of internal pressure at failure [43].

3.6 Conclusions

This study aims to use the XFEM to simulate the fracture of API 5L X52 grades of X52 vintage pipes with circumferential flaws under the effect of internal pressure and eccentric tension loading. The maximum principal strain and fracture energy were chosen as the damage parameters in the XFEM simulation. Appropriate values for these damage parameters were obtained by a comprehensive comparison with eight full-scale experimental test results. The comparison included tensile strain, CMOD, applied load, and rotation at end plates. The XFEM results indicated that appropriate damage parameters of maximum principal strain of 0.085 and fracture energy of 900 kN/mm can be used to replicate the experimental results. The comparisons of the numerical and experimental results of tensile strain capacity along the pipe length showed good agreement. The XFEM models satisfactorily predicted the tensile strain along the pipe length using the proposed fracture properties. Regardless of the differences in the pipe and crack dimensions as

39

well as the internal pressure of each model, the XFEM analysis can accurately predict the initiation and propagation of the crack in all eight models. The XFEM predicted results of CMOD-applied force and rotation-force were also compared with test results and good agreement was observed. Models 5 and 6, characterized by shallow and long cracks, exhibited a slightly more ductile behaviour. For these two models, the maximum principal strain of 0.2 and fracture energy of 900 N/mm produced a model with a better match of the experimental results of tests 5 and 6. This difference can be justified due to the existence of multiple crack fronts or the natural variability associated with fracture, which both lead to higher fracture energy and eventually higher tensile strain capacity. Similar to the experimental study of the crack surface, the XFEM analysis of the crack surface suggests a brittle fracture in X52 grades of pipeline. Future work will focus on obtaining the damage parameters of the X52 grade of pipeline in small-scale tests. Analysis of the fracture response in both small-scale and full-scale tests will help to better predict the material damage parameters considering the impact of the base metal fracture toughness and the weld metal structure and will lead to developing a tensile strain equation that can predict the TSC for this grade of vintage pipeline.
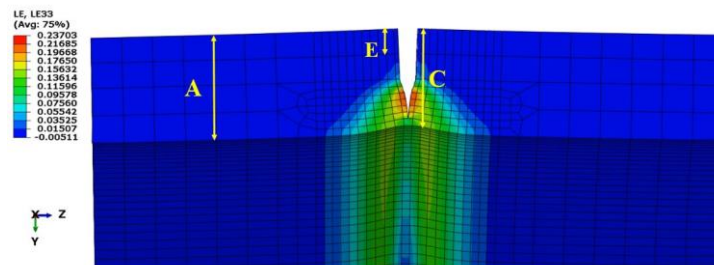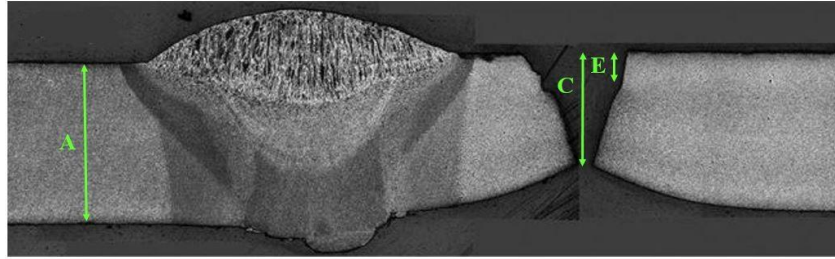
Figure 3.13 Geometry of fracture location at failure in the longitudinal direction from (a) Model 1 and (b) Test 1 [58].

Chapter 4: Strain-based XFEM prediction of crack propagation in single edge notched tension (SENT) tests

This chapter will be submitted as a journal article to a peer-reviewed journal.

4.1 Abstract

In the present study, the use of the extended finite element method (XFEM) to predict the fracture response of the X42 vintage pipeline material is investigated. A set of damage parameters in the cohesive zone model (CZM) which are the maximum principal strain (Maxpe) and fracture energy (G_c), previously obtained from simulation of full-scale tests is used. The side-grooved single edge notched tensile (SENT) model for X42 grade of pipe is simulated. The predicted XFEM force to crack mouth opening displacement (CMOD) and crack tip opening displacement (CTOD) to crack extension results were compared with the experimental SENT results. The force to CMOD results indicate that the XFEM is a useful method to simulate the crack propagation in the X42 SENT model. However, CTOD to crack extension results recommend the calibration of the XFEM damage criterion using both small-scale and full-scale tests to ensure the accuracy in prediction of damage response for this grade of pipeline material.

4.2 Introduction

The worldwide need for natural gas and petroleum has considerably increased in the last decade [60–62]. Therefore, the importance of the capability of pipelines to withstand large plastic deformations in a harsh environment is required [63–65]. Strain-based design (SBD) is a practical method in designing pipelines that can withstand considerable plastic deformation in severe environments [66]. In order to develop the SBD approach, proper fracture mechanics tests are useful in predicting the strain capacity of pipeline material. The single edge notched tensile (SENT) test is considered an effective experimental test to assess tensile fracture resistance in

pipelines [67,68], primarily due to the similarity between the constraint conditions of the tip of the crack in SENT tests with actual flaws in girth welds of pipelines [66]. Additionally, crack tip opening displacement (CTOD)-crack extension curves obtained from SENT experiments are similar to those obtained from full-scale tests [42].

Due to the intricate details and the required precision, small-scale SENT can be costly. Full-scale experiments are also associated with exuberant costs, due to the need for providing external forces or internal pressure as a part of the experiments as well as initial cracks. Elasto-plastic fracture modelling techniques can help to reduce the required number of such tests and ultimately, the total cost by calibrating models that are capable of predicting the damage mechanism and modeling the initiation and propagation of cracks under complicated loading conditions [42]. The extended finite element method (XFEM) is one of the most effective methods in modeling ductile fracture mechanics. In this method, the initiation and propagation of the crack can be simulated without the need to remesh the area near the tip of the crack, which leads to a decrease in the time of simulation in comparison with time consuming mesh generation near crack location need in traditional FEM [31,69,70] .

XFEM is a powerful tool in predicting the ductile damage properties of both full-scale tests for pipes and small-scale experiments such as SENT tests [42]. This method has been widely used recently for predicting the fracture response in pipeline. Zhang et al. [71] used XFEM to predict the failure of three-dimensional (3D) cracks-in-corrosion flaws in X60 grades of the pipeline using maximum principal strain (Maxpe) and fracture energy (G_c) as the damage criteria. Lin et al. [43] used a maximum principal stress (Maxps)-based damage criterion combined with G_c in an XFEM model to predict the fracture behavior of the X52 vintage pipe and satisfactorily compared it with

eight full-scale experiments. Similarly, Elyasi et al. [72] investigated the fracture response of X52 vintage pipeline using the strain-based damage set comprised of Maxpe of 0.085 and G_c of 900N/mm, and calibrated the predicted tensile strain capacity (TSC) results with full-scale experiments of cracked pipeline under internal pressure and bending.

Agbo et al. [5] obtained Maxpe and G_c required in the XFEM simulation of X42 vintage pipeline as well as the TSC through the calibration with full-scale experimental result and demonstraded the ability of the proposed XFEM model to analyze the effect of flaw size and internal pressure on TSC. Ameli et al. [42] used the XFEM model of the SENT test of X42 vintage pipe using calibrated damage parameters, Maxps and G_c, to predict the ductile fracture behavior of this grade of vintage pipeline. The mesh sensitivity analysis presented by Ameli et al. [42] demonstrated the importance of mesh size on the tearing and fracture behavior for crack extension. Okodi et al. [41] used Maxpe and G_c as damage criteria to simulate the propagation of cracks in X60 pipe grade. They calibrated the XFEM results using SENT experiments from full-scale tests and predicted the burst pressure in pipes with different size of external cracks.

To Summarize the recent work, Ameli et al. [42] used a maximum principal stress-based (Maxps) approach in XFEM analysis of X42 vintage pipes. Critical Maxpe values were related to the critical experimental strain values obtained in the surrounding area of a crack tip, suggesting that Maxpe may be a more suitable damage criterion compared to Maxps [5]. Subsequently, Agbo et al. [5] obtained the strain-based damage parameters for X42 steel pipe in the full-scale XFEM analysis. However, there is a need to investigate whether the damage parameters proposed by Agbo et al [5] from full-scale tests, provide the same prediction for the small-scale experimental results obtained by Ameli et al. [42,73]. This paper aimed to investigate the validation of the XFEM

44

analysis in predicting the initiation and propagation of the crack in the SENT test of ductile X42 vintage pipe. The validation of the damage parameters (Maxpe and G_c), which were previously obtained for full-scale tests, were examined for the SENT model by comparing the predicted XFEM results with SENT test. The comparisons are in terms of force-CMOD (crack mouth opening displacement) and CTOD-crack extension.

4.3 Experimental tests of SENT specimens

The SENT tests were carried out on specimens that were cut from X42 vintage pipe material [42,73]. The specimens were machined to have a thickness (B) and width (W) of equal dimensions (12 mm). The total length and gripping length (H) were 374 mm and 120 mm (10×W), respectively (Figure 4.1). The initial notch with a radius of 0.075 mm was carved using electrical discharge machining (EDM) on the square cross-section of the specimens (B×W). Also, side grooves equal to 5% of sample thickness were manufactured on all sides of the SENT sample. The ratio of the crack depth (a in Figure 4.1) to width (W) was equal to 0.33. The schematic view of the SENT specimen is illustrated in Figure 1 [73].
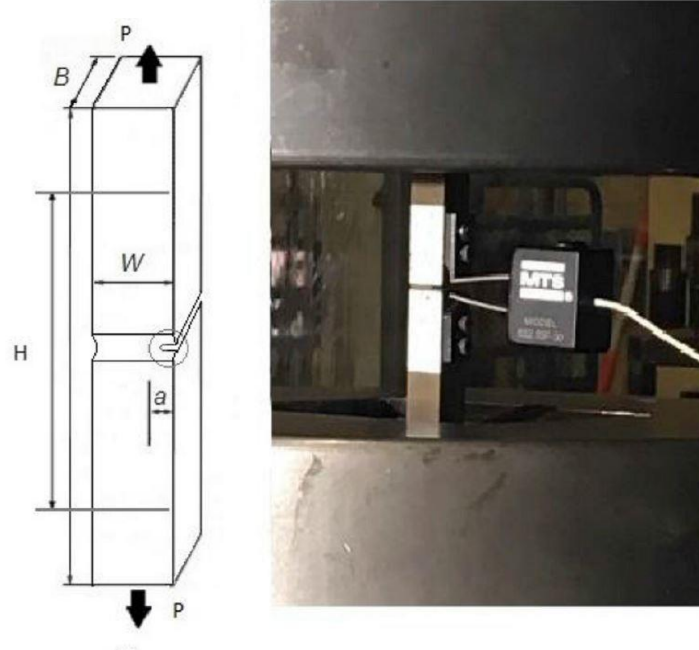
Figure 4.1 Schematic view of SENT specimen geometry subject to a tension test (a) and a SENT test specimen instrumented with a clip gauge and knife edges (b) [42].

In the first step, both ends of the SENT samples were clamped and subjected to tensile force (marked as "P" in Figure 4.1) with a constant loading rate of 0.01 mm/s. To allow calculation of the cack extension, the loading was stopped before failure occurred in the load-displacement curves. The original and final crack profiles were determined through microscopic studies of the crack surfaces and the average technique and the nine-point measurement were used to obtain the crack profiles [74]. To determine the CTOD, the digital image correlation (DIC) system constantly monitored the movement of two nodes located 2.5 mm above and below the initial crack tip during the test (Figure 4.2).
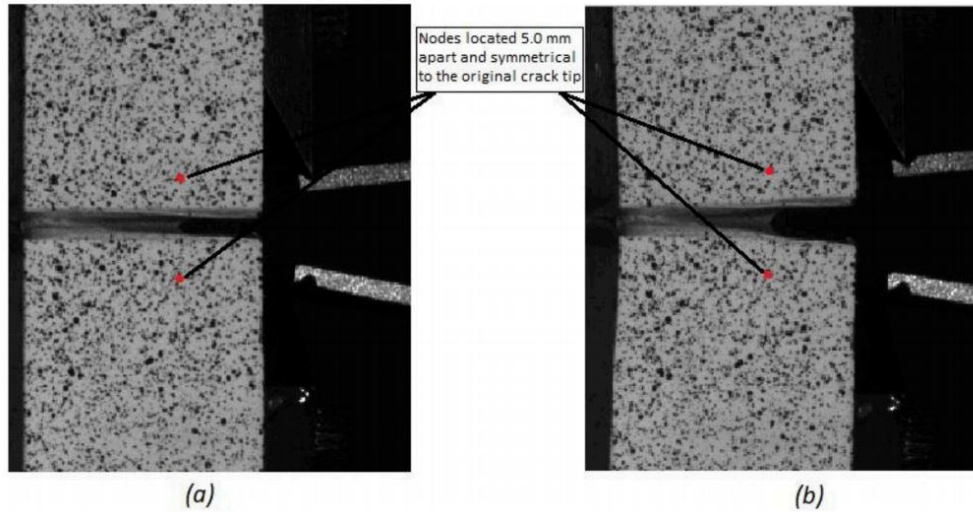
Figure 4.2 Location of nodes 2.5 mm above and below the initial crack tip at (a) first and (b) final loading steps [42].

According to the standard for SENT tests**,** the crack was allowed to propagate a maximum length of 2 mm. Also, due to initial inspection and blunting, the calculated crack growth below 0.2 mm could not be used for curve fitting [42]. The CTOD-Δa (crack extension) experimental results for the X42 SENT tests obtained in Ameli et al. [73] were used in the current study using the fracture parameters obtained by Agbo et al. [5].

Clip gauges were mounted by two knife edges to the SENT sample to accurate gauging the CMOD (Figure 4.3). The distance between two clips as well as measured CTOD were used to calculate the CMOD in the following equation [73]:

$$\text{CMOD} = \frac{\text{CTOD} \times h_1 + V_1 \times (a_0)}{(a_0 + h_1)} \qquad 4.1$$

where h_1 was the height of clip gauge, V_1 was distance between two clip gauges, and a_0 was the initial crack depth, which are shown in Figure 4.3. Calculated CMODs and corresponding forces

measured by the tension machine were used to obtain the force-CMOD curves for the X42 SENT

samples as described by Ameli et al. [73].

<center>(a)   (b)</center>
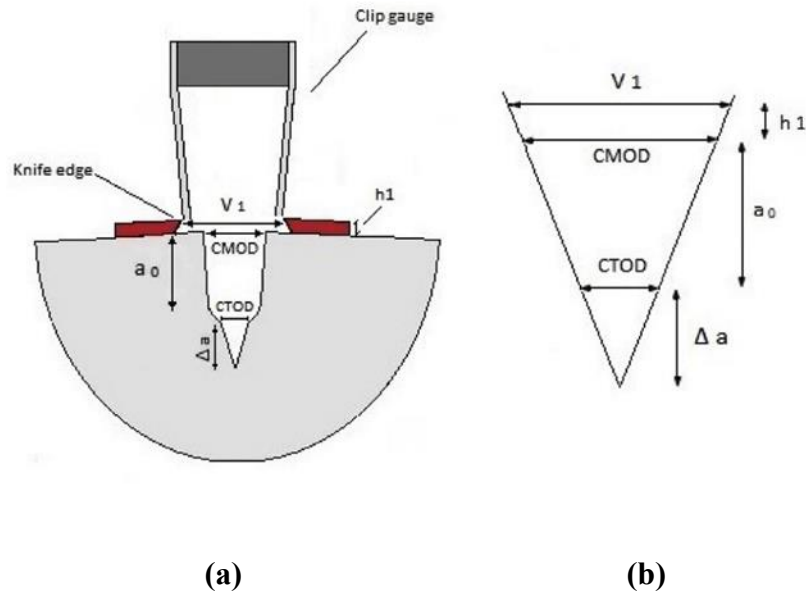
Figure 4.3 Crack extension profile (a) and CMOD measurement parameters (b) [73].

4.4 XFEM Model

In this study, the strain-based damage parameters, Maxpe and G_c were 0.013 and 450 N/mm

respectively obtained from Agbo et al. [5] after calibrating an XFEM model for predicting the

tensile strain capacity of full scale X42 experimental tests. The 3D XFEM model was simulated

using ABAQUS/Standard (v. 6.17) [59]. The tensile properties of the pipe were taken from the six

true stress-strain curves obtained from the tension test carried out on X42 pipe specimens by Ameli

et al. [73]. The material properties used in the XFEM model are shown in Table 4.1.

Table 4.1 Material properties of the X42 pipe [73].

Young's modulus (GPa)	Poisson's ratio	0.2% Offset yield strength (MPa)	Ultimate tensile strength (MPa)
200	0.3	314	640

Figure 4.4 shows the finite element (FE) configuration and boundary conditions of the SENT model containing the crack. To reduce the analysis time and the computational effort, only half of the SENT sample was modeled by taking advantage of the symmetry of the model around the YZ plane (Figure 4.4).

The XFEM crack was modeled as a shell planar part and located in the middle height of the SENT model (Figure 4.4). The XFEM SENT model was meshed by the 8-node linear brick, reduced integration, hourglass control element (C3D8R). The mesh size was 4 mm along the crack propagation route. To reduce the simulation time, a coarser mesh was used for the elements far from the crack propagation route. Mesh convergence analysis was performed to guarantee the accuracy of the analysis, which will be discussed later in this study. To simulate the tension test leading to crack initiation and propagation, the external displacement of 50 mm was applied on the reference node represented in Figure 4.4(b) as a boundary condition in the Y direction.

4.5 Data analysis

The CMOD-force results were obtained from XFEM analysis and compared with the experiments obtained by Ameli et al. [73]. Since the failure in the X42 vintage pipeline occurred in the weld metal [5], only the experiments from weld material were represented for the comparison. Also, damage parameters (Maxpe of 0.013 and G_c of 450 N/mm) were used in the current XFEM analysis, obtained for the weld metal part of the X42 pipeline by Agbo et al [5]. The CMOD was

calculated by subtraction of the displacement in y-direction (U_y) of the two points shown in Figure 4.5. The applied force in the y-direction was extracted from the reference points shown in Figure 4.4.

(a)

(b)
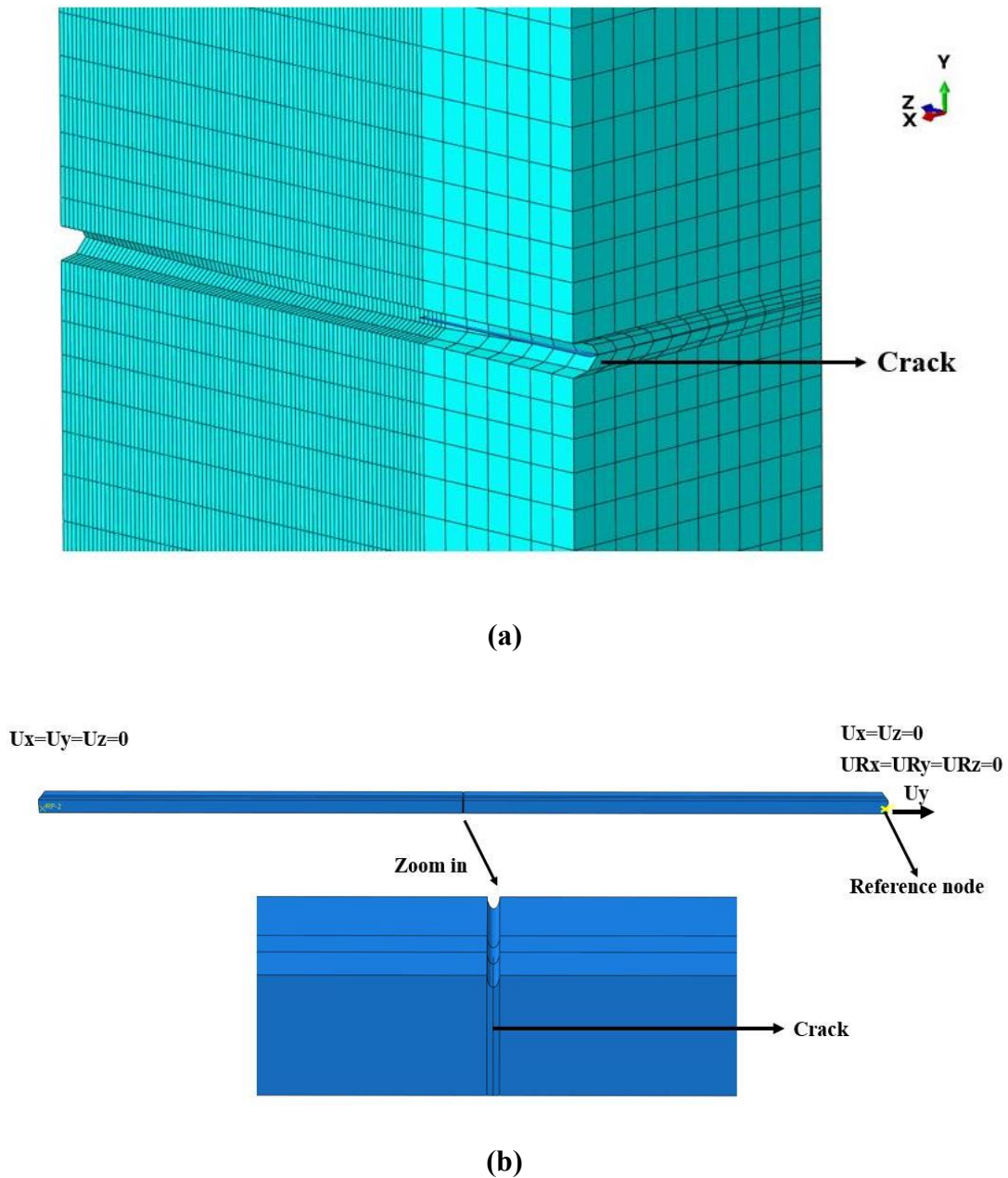
Figure 4.4 FE configuration of the symmetric SENT model (a) the location of the crack in the middle height of the specimen, (b) boundary conditions of the specimen.

50

The CTOD-crack extension results from the XFEM analysis were calculated and compared with the experimental results obtained by Ameli et al. [73]. The CTOD values were obtained using two different approaches of crack extension and presented in Figure 4.6. First, the crack extension was calculated based on the propagation of the crack-tip point through the thickness of the SENT model (Figure 4.6. (a)). In this approach, crack extension was calculated by monitoring the crack tip. This method was also applied by Ameli et al. [42,73] in obtaining crack extension in experimental and XFEM results. In the second approach, the crack extension was extracted based on the propagation of the damaged element, which was defined when status in ABAQUS XFEM (STATUSXFEM) for an element equals 1 (Figure 4.6(b)). In this approach, the crack extension was obtained when the full separation occurred (STATUSXFEM=1) between two elements aligned with the crack propagation route. Figure 4.6(a) and (b) represented the status of the damaged element and the crack extension in both approaches at a crack tip extension of 1.6 mm.
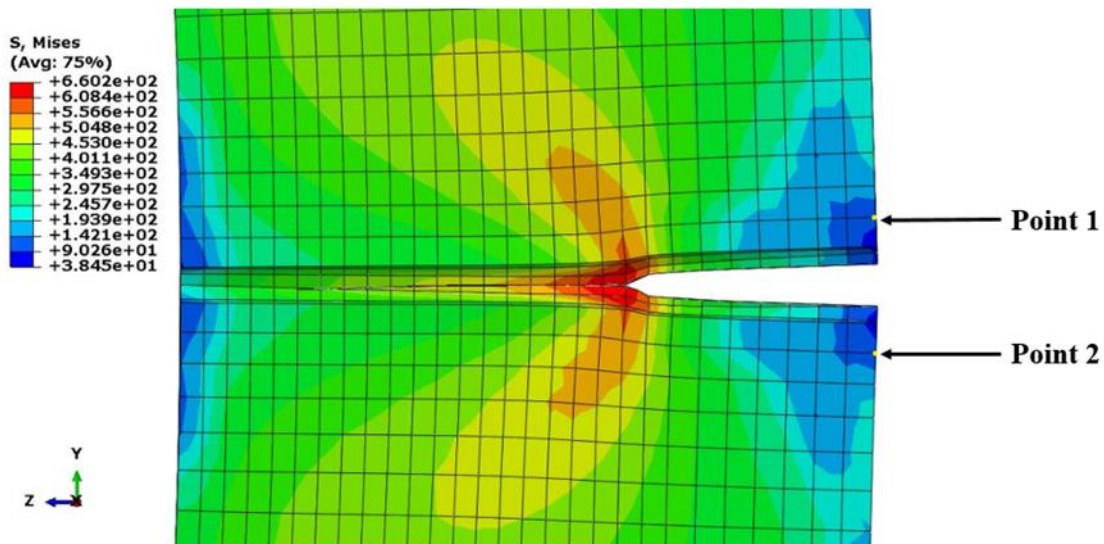
Figure 4.5 The initiation and propagation of the crack in the XFEM SENT model and selected points in calculating CMOD.

51

It can be observed that the damage did not occur in the elements aligned with the crack propagation route in the crack tip extension approach since STATUSXFEM<1 in these elements (Figure 4.6(a)). On the other hand, the crack extension based on the damaged element propagation approach showed that the failure happened (STATUSXFEM=1) in elements along the crack extension line (Figure 4.6(b)). The results showed that at the same crack extension, CTOD was higher in the damage element approach in comparison with the crack tip approach.

4.6 Results

The comparison of the CMOD-force curves of the XFEM models with experiments is illustrated in Figure 4.7. As observed, the numerical results compared well with experiments, underscoring the capability of XFEM in predicting the fracture behavior of the modelled specimens.
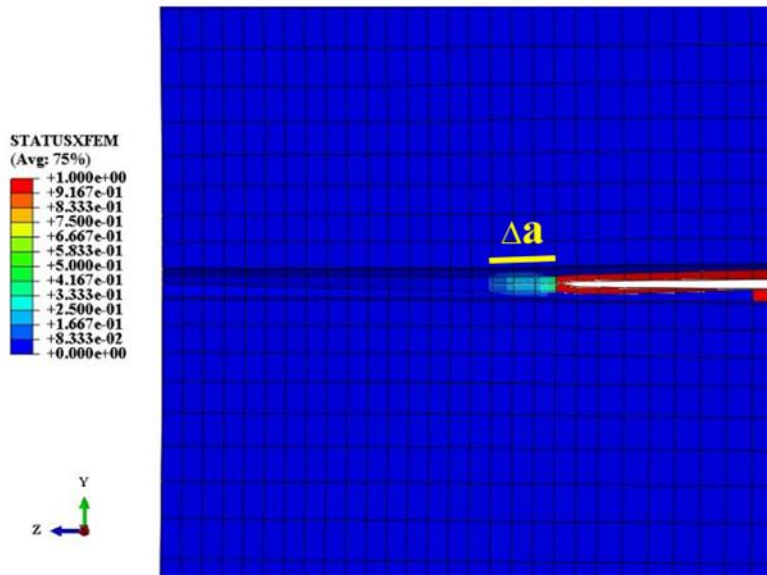
(a)
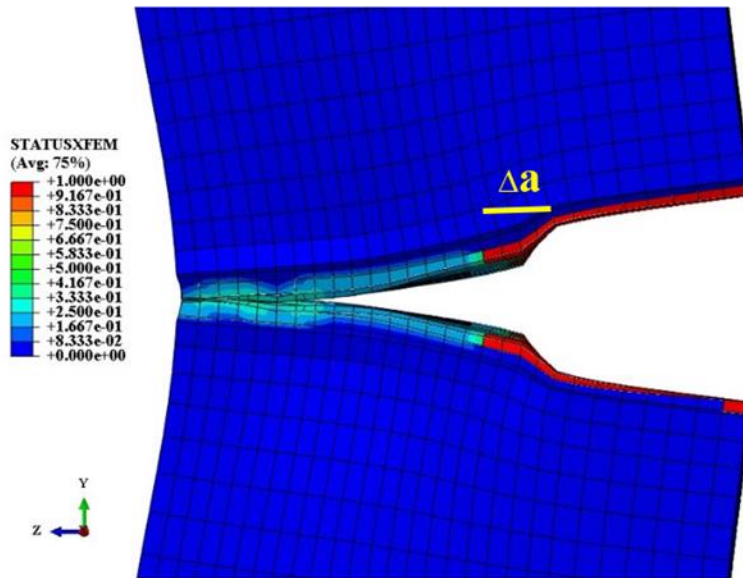
(b)

Figure 4.6 The crack extension (Δa) based on propagation of (a) the crack tip (b) STATUSXFEM=1.
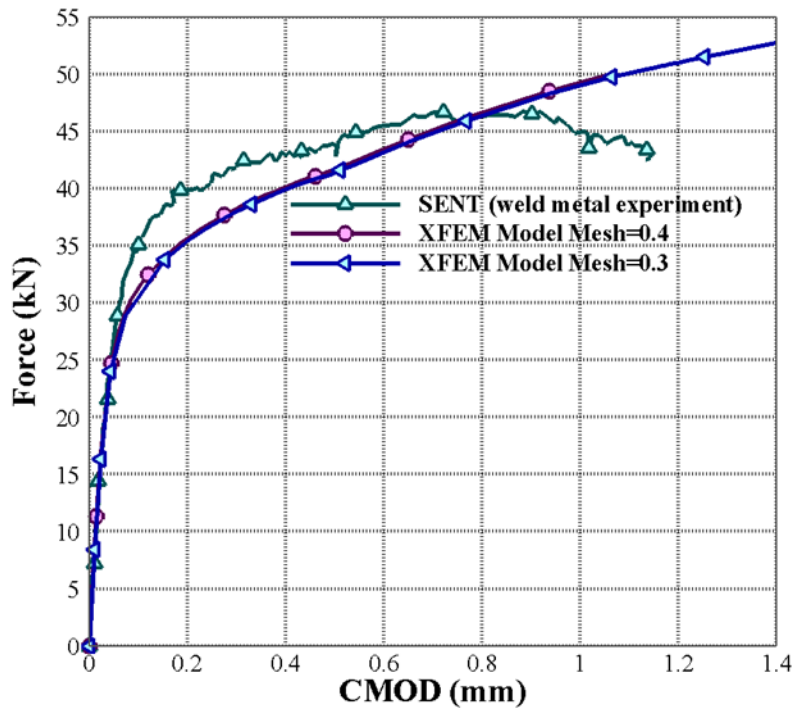
Figure 4.7 Comparison of CMOD-force from XFEM analysis with experiments from Ameli et al. [73].

53

The mesh sensitivity investigation was performed to obtain the optimum element size needed for accuracy of the analysis. Two different element sizes aligned with the crack propagation route were applied; 0.3 mm and 0.4 mm. As observed in Figure 4.7, the results obtained using the element sizes 0.3 mm and 0.4 mm are similar while 0.4 mm element size provides the results with less computational efforts. Therefore, the optimum element size of 0.4 mm was chosen to ease the computational cost without sacrificing the accuracy.

The CTOD-crack extension curves obtained through both crack-extension approaches are calibrated by comparing them with the experimental results obtained by Ameli et al. [73] and presented in Figure 4.8. Similar to the CMOD-force curves, there was no significant difference in the predicted CTOD values using mesh sizes of 0.3 mm and 0.4 mm, and an optimized mesh size of 0.4 mm was selected to reduce the simulation time.

The results showed that the predicted CTODs underestimated the test results when the crack extension was calculated based on the propagation of the crack tip (first crack extension criterion). On the other hand, the predicted CTOD results were higher than the experiments when propagation of the damaged element was the full separation (STATUSXFEM=1) crack extension criterion. It can be concluded that the best results were aligned somewhere between the two predicted results. This ratio of two predicted results, which can present the best results in calibration with the experiments was obtained as follows:

$$\frac{\text{CTOD (crack tip approach)}}{\text{CTOD (damaged element approach)}} = 3 \tag{2}$$
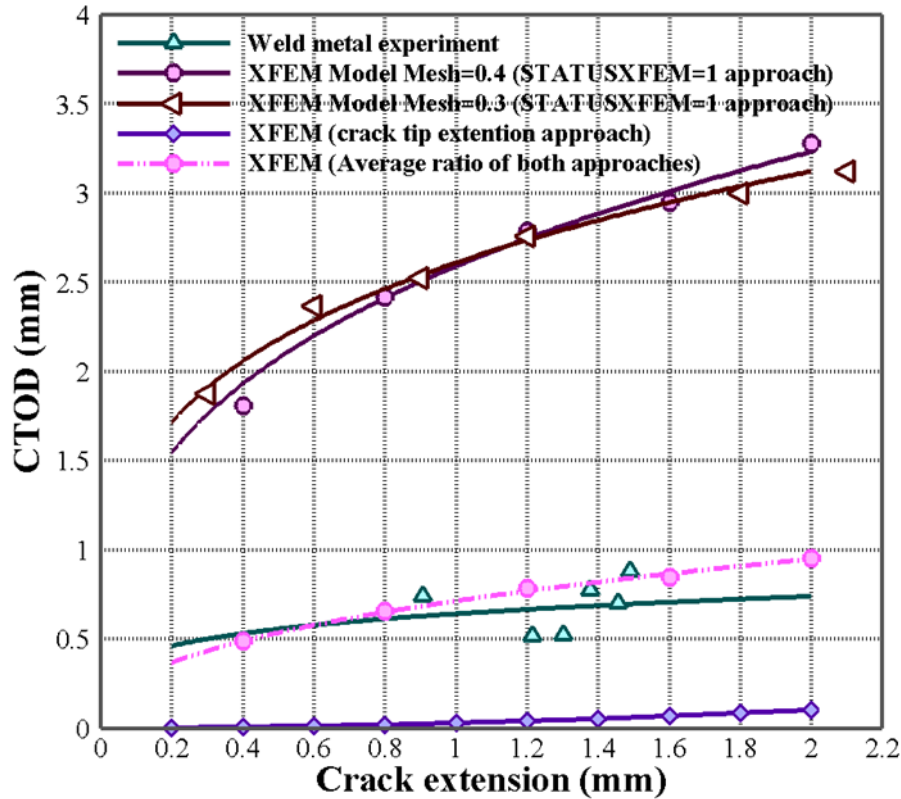
Figure 4.8 Comparison of CTOD-crack extension (Δa) from XFEM analysis with experiments results from Ameli et al. [73].

4.7 Discussion

The results from the current XFEM were capable of representing the crack propagation correctly in 3D analysis, as shown in Figure 5. Also, the fracture parameters, Maxpe of 0.013 mm/mm and Gc of 450 N/mm, showed good predictions of tensile strain along the pipe length and CMOD-applied moment curves in comparison with the full-scale experiments [5]. XFEM parameters can seemingly be calibrated from either full-scale or small-scale tests. The obtained damage parameters for X42 pipeline material from full-scale experiments can calibrate the CMOD-force curves of SENT tests accurately (Figure 4.7), but showed poor predictions in calibration of the CTOD-crack extension results (Figure 4.8). These comparisons highlight the need for further

55

research in the relationship between calibration of XFEM parameters using small-scale and full-scale tests.

An explanation for differences between the CTOD-crack extension curves could be the different location of the crack tip between the experimental test and XFEM simulation. Ameli et al. [42] obtained the crack tip extension by monitoring the crack tip using a digital image correlation system during the SENT test. The propagation of the crack tip in XFEM analysis happened when the Maxps in the integration point located near the tip of the crack exceeded the tensile strength of the material [75]. As a result, XFEM predictions of CTOD-crack extension were different from the experimental results.

4.8 Conclusion

This study investigated the capability of XFEM in simulating the initiation and propagation of the SENT model for X42 pipeline materials. The XFEM fracture parameters: maximum principal strain and fracture energy were 0.013 and 450 N/mm respectively, as previously obtained by Agbo et al. [5] through simulating the full-scale tests of X42 pipe. These parameters were applied to simulate fracture propagation in the SENT tests conducted by Ameli et al. [42,73]. Our work shows that XFEM can accurately simulate the propagation of cracks in the SENT model and can succeessfully replicate the CMOD-force results. The accuracy of the numerical CTOD-crack extension results, however, are dependent on the identification of the crack tip in the model. Two different "physical crack tip" definitions based on two extremes were used. The first assumes the physical crack tip to be at the location of damage initiation and the second assumes the physical crack tip to be at the location of complete separation. The "physical crack tip" that precipitated in the best match between the experiments and the simulation was found to be the weighted average

of the two predicted results, in which the weight of CTODs obtained at the tip of the crack to those obtained from damaged element was 3.0/1.0. Future work will investigate the relationships between the damage parametes obtained from small-scale and full-scale models in various pipeline grades in addition to properly defining the most appropriate "physical crack tip" in small-scale tests.

Chapter 5: Conclusion

This research investigated the capability of the strain-based design to predict crack propagation in small-scale and full-scale tests. First, the XFEM analysis was applied to model the full-scale tests from Abdulhameed et al. [58] and Lin [16]. The eight XFEM models of X52 pressurized vintage pipe were developed in ABAQUS software to predict fracture behavior of X52 grade of pipelines. The set of damage parameters included maximum principal strain (Maxpe) of 0.085 and fracture energy (G_c) of 900 N/mm used in the XFEM model of the full-scale pipes to simulate the initiation and propagation of the crack. The XFEM models were capable to reproduce the experiments properly. The comparisons were investigated in terms of tensile strain values along pipe length, CMOD-force, as well as rotation-applied force between XFEM and tests. In the next step in the current research, XFEM models of the single edge notched tension (SENT) test of the X42 vintage pipelines were calibrated using the experiments to investigate whether the XFEM analysis was robust in the prediction of the fracture response in small-scale tests as well. The results suggested the strain-based fracture properties of X42 (Maxpe=0.013, G_c=450 N/mm), which successfully predicted the results of full-scale tests in previously published results by Agbo et al. [5], could properly simulate the initiation and propagation of the crack in the 3D XFEM model and validate the CMOD-force experimental results as well but showed poor prediction in reproducing the CTOD-crack extension from the tests. The results raise the question of whether the XFEM damage properties, which successfully simulated the full-scale test, have a similar trend in predicting the small-scale test results too. The results suggested that the future work in the analysis of the damage response of vintage steel pipelines should first focus on the XFEM calibration process of the small-scale tests before the analysis of the full-scale tests to ensure the accuracy of obtained damage properties.

References

[1]   Wikipedia.org/wiki/Trans-Alaska_Pipeline_System#/media/File:Trans-Alaska_Pipeline_System_Luca_Galuzzi_2005,.

[2]   M. Paredes, C. Ruggieri, Engineering approach for circumferential flaws in girth weld pipes subjected to bending load, Int. J. Press. Vessel. Pip. 125 (2015) 49–65. https://doi.org/https://doi.org/10.1016/j.ijpvp.2014.09.003.

[3]   S. Agbo, M. Lin, I. Ameli, A. Imanpour, D.-M. Duan, J.J.R. Cheng, S. Adeeb, Experimental evaluation of the effect of the internal pressure and flaw size on the tensile strain capacity of welded X42 vintage pipelines, Int. J. Press. Vessel. Pip. 173 (2019) 55–67. https://doi.org/10.1016/J.IJPVP.2019.04.010.

[4]   B. Liu, X.J. Liu, H. Zhang, Strain-based design criteria of pipelines, J. Loss Prev. Process Ind. 22 (2009) 884–888. https://doi.org/10.1016/j.jlp.2009.07.010.

[5]   S. Agbo, M. Lin, I. Ameli, A. Imanpour, D.M. Duan, J.J.R. Cheng, S. Adeeb, Evaluation of the effect of internal pressure and flaw size on the tensile strain capacity of X42 vintage pipeline using damage plasticity model in extended finite element method (XFEM), in: Am. Soc. Mech. Eng. Press. Vessel. Pip. Div. PVP, American Society of Mechanical Engineers (ASME), 2019: pp. PVP2019--94005, V005T05A006; 9 pages. https://doi.org/10.1115/PVP2019-94005.

[6]   D. Jia, Y.-Y. Wang, S. Rapp, Material Properties and Flaw Characteristics of Vintage Girth Welds, (2020). https://doi.org/10.1115/IPC2020-9658.

[7]   Y.-Y. Wang, D. Horsley, S. Rapp, Evolution of Linepipe Manufacturing and its
        Implications on Weld Properties and Pipeline Service, in: Proceedings of the International
        Pipeline Conference, Calgary, Alberta, Canada, 2016: pp. 26–30.
        https://doi.org/10.1115/ipc2016-64632.

[8]   API Specification 5L (2012). Specification for line pipe (45th ed.)., Washington,
        DC:American Petroleum Institute (AIP), 2012. https://infostore.saiglobal.com/en-
        us/Standards/API-5L-2012-96281_SAIG_API_API_201493/.

[9]   H. Gao, Z. Yu, Z. Zhang, H. Shi, The concepts for pipeline strain-based design, in: Proc.
        Seventeenth Int. Offshore Polar Eng. Conf., Lisbon, Portugal, 2010: pp. 476–482.
        https://www.onepetro.org/conference-paper/ISOPE-I-10-218 (accessed August 31, 2020).

[10]   S. Barbas, M. Weir, Strain-based design methodology for seismic and arctic regions, in:
        Proc. Seventeenth Int. Offshore Polar Eng. Conf., Lisbon, Portugal, 2007: pp. 3073–3080.
        https://www.onepetro.org/conference-paper/ISOPE-I-07-535 (accessed August 31, 2020).

[11]   E.S. Drexler, A.J. Slifka, D.S. Lauria, M.J. Connolly, R.L. Amaro, The Effect of
        Pressurized Hydrogen Gas on the Fatigue Properties of Welds in X52 and X70 Pipelines,
        (2016).

[12]   D.G. Stalheim, K.R. Barnes, D.B. Mccutcheon, Alloy designs for high strength oil and gas
        transmission linepipe steels, in: Proc. Int. Symp. Microalloyed Steels Oil Gas Ind.,
        CBMM/TMS, 2006: pp. 73–108.

[13]   D. Stalheim, L. Hayden, Metallurgical considerations for commercial steels used for
        hydrogen service, in: Proc. 2008 Int. Hydrog. Conf., 2009: pp. 332–340.

[14]   Y.F. Cheng, Stress Corrosion Cracking of Pipelines, John Wiley & Sons, Inc., Hoboken, NJ, USA, 2013. https://doi.org/10.1002/9781118537022.

[15]   A.J. Slifka, E.S. Drexler, D.G. Stalheim, R.L. Amaro, D.S. Lauria, A.E. Stevenson, L.E. Hayden, The effect of microstructure on the hydrogen-assisted fatigue of pipeline steels, in: Am. Soc. Mech. Eng. Press. Vessel. Pip. Div. PVP, American Society of Mechanical Engineers Digital Collection, Paris, France, 2013: pp. PVP2013-97217, V06BT06A009. https://doi.org/10.1115/PVP2013-97217.

[16]   M. Lin, Characterization of tensile and fracture properties of X52 steel pipes and their girth weld [MSc thesis], University of Alberta, Edmonton, AB, Canada, 2015. https://doi.org/10.7939/R3X05XM68.

[17]   Failure Modes in Pressurised Pipeline Systems | Water Services Association of Australia, 2012. https://www.wsaa.asn.au/shop/product/8691 (accessed March 18, 2021).

[18]   S.. Kailas, Failure. Class lecture for course Material Science. Indian Institute of Science, Bangalore, India., n.d. https://nptel.ac.in/courses/112/108/112108150/ (accessed August 6, 2020).

[19]   D.R. Askeland, P.P. Phule, The Science and Engineering of Materials, Fifth Edit, Thomson, Toronto, 2006. https://doi.org/10.1080/03043799408928327.

[20]   J.R. Davis, Tensile Testing, 2nd Edition, ASM International, 2004. https://www.asminternational.org/search/-/journal_content/56/10192/05106G/PUBLICATION (accessed August 6, 2020).

[21]   T.L. Anderson, Fracture Mechanics: Fundamentals and Applications, Third Edition, 3rd

        ed, Boca Raton, FL: Taylor & Francis Group., 2005.

        https://doi.org/10.1201/9781420058215.

[22]   H. Czichos, T. Saito, L. Smith, Springer handbook of materials measurement methods,

        2006. https://link.springer.com/978-3-540-20785-6 (accessed September 8, 2020).

[23]   B. Bhushan, Principles and Applications of Tribology, 2nd Edition, John Wiley & Sons,

        New York, 2013. https://www.wiley.com/en-

        us/Principles+and+Applications+of+Tribology%2C+2nd+Edition-p-9781118403013

        (accessed September 9, 2020).

[24]   A.T. Zehnder, Fracture Mechanics, 1st ed., Springer Netherlands, 2012.

        https://doi.org/10.1007/978-94-007-2595-9_1.

[25]   D. Gross, T. Seelig, Fracture Mechanics: With an Introduction to Micromechanics,

        Springer, Troy, NY, 2006. https://www.amazon.ca/Fracture-Mechanics-Micromechanics-

        Dietmar-Gross/dp/3540240349 (accessed September 11, 2020).

[26]   S.K. Chan, I.S. Tuba, W.K. Wilson, On the finite element method in linear fracture

        mechanics, Eng. Fract. Mech. 2 (1970) 1–17. https://doi.org/https://doi.org/10.1016/0013-

        7944(70)90026-3.

[27]   P. Vazouras, S.A. Karamanos, P. Dakoulas, Finite element analysis of buried steel

        pipelines under strike-slip fault displacements, Soil Dyn. Earthq. Eng. 30 (2010) 1361–

        1376. https://doi.org/https://doi.org/10.1016/j.soildyn.2010.06.011.

[28] Y.S. Hsu, Finite element approach of the buried pipeline on tensionless foundation under random ground excitation, Math. Comput. Simul. 169 (2020) 149–165. https://doi.org/https://doi.org/10.1016/j.matcom.2019.09.004.

[29] Z. Zhang, X. Ni, Y. Frank Cheng, Assessment by finite element modelling of the mechano-electrochemical interaction at double-ellipsoidal corrosion defect with varied inclinations on pipelines, Constr. Build. Mater. 260 (2020) 120459. https://doi.org/https://doi.org/10.1016/j.conbuildmat.2020.120459.

[30] J. Chen, H. Wang, M. Salemi, P.N. Balaguru, Finite Element Analysis of Composite Repair for Damaged Steel Pipeline, Coatings . 11 (2021). https://doi.org/10.3390/coatings11030301.

[31] N. Sukumar, N. Moes, B. Moran, T. Belytschko, Extended finite element method for three-dimensional crack modelling, Int. J. Numer. Methods Eng. 48 (2000) 1549–1570. https://doi.org/10.1002/1097-0207(20000820)48:11<1549::AID-NME955>3.0.CO;2-A.

[32] E. Maire, C. Bordreuil, L. Babout, J.-C. Boyer, Damage initiation and growth in metals. Comparison between modelling and tomography experiments, J. Mech. Phys. Solids. 53 (2005) 2411–2434. https://doi.org/https://doi.org/10.1016/j.jmps.2005.06.005.

[33] A. Pineau, Development of the local approach to fracture over the past 25 years: theory and applications, Int. J. Fract. 138 (2006) 139–166.

[34] A. Alvaro, V. Olden, O.M. Akselsen, 3D cohesive modelling of hydrogen embrittlement in the heat affected zone of an X70 pipeline steel–Part II, Int. J. Hydrogen Energy. 39 (2014) 3528–3541.

[35] S. Parmar, C. Bassindale, X. Wang, W.R. Tyson, S. Xu, Simulation of ductile fracture in pipeline steels under varying constraint conditions using cohesive zone modeling, Int. J. Press. Vessel. Pip. 162 (2018) 86–97.

[36] N. Bonora, D. Gentile, A. Pirondi, Identification of the parameters of a non-linear continuum damage mechanics model for ductile failure in metals, J. Strain Anal. Eng. Des. 39 (2004) 639–651. https://doi.org/10.1243/0309324042379356.

[37] S. Ma, H. Yuan, A continuum damage model for multi-axial low cycle fatigue of porous sintered metals based on the critical plane concept, Mech. Mater. 104 (2017) 13–25. https://doi.org/https://doi.org/10.1016/j.mechmat.2016.09.013.

[38] F. Shen, S. Münstermann, J. Lian, Investigation on the ductile fracture of high-strength pipeline steels using a partial anisotropic damage mechanics model, Eng. Fract. Mech. 227 (2020) 106900. https://doi.org/https://doi.org/10.1016/j.engfracmech.2020.106900.

[39] N. Moës, J. Dolbow, T. Belytschko, A finite element method for crack growth without remeshing, Int. J. Numer. Methods Eng. 46 (1999) 131–150. https://onlinelibrary.wiley.com/doi/abs/10.1002/(SICI)1097-0207(19990910)46:1%3C131::AID-NME726%3E3.0.CO;2-J?casa_token=Uc9Gtwo1LroAAAAA:TtFKISmE71Jqd5Qp78Nl4AM7H078rwkvIAREm lFD6vK4dqhnil2YvRQ_M8F8Xs7lK-_6FX8Dp5XdvS4.

[40] E. Giner, N. Sukumar, J.E. Tarancón, F.J. Fuenmayor, An Abaqus implementation of the extended finite element method, Eng. Fract. Mech. 76 (2009) 347–368. https://doi.org/10.1016/j.engfracmech.2008.10.015.

[41]   A. Okodi, M. Lin, N. Yoosef-Ghodsi, M. Kainat, S. Hassanien, S. Adeeb, Crack propagation and burst pressure of longitudinally cracked pipelines using extended finite element method, Int. J. Press. Vessel. Pip. 184 (2020) 104115. https://doi.org/10.1016/j.ijpvp.2020.104115.

[42]   I. Ameli, B. Asgarian, M. Lin, S. Agbo, R. Cheng, D. ming Duan, S. Adeeb, Estimation of the CTOD-crack growth curves in SENT specimens using the eXtended finite element method, Int. J. Press. Vessel. Pip. 169 (2019) 16–25. https://doi.org/10.1016/j.ijpvp.2018.11.008.

[43]   M. Lin, S. Agbo, D.-M. Duan, J.J.R. Cheng, S. Adeeb, Simulation of Crack Propagation in API 5L X52 Pressurized Pipes Using XFEM-Based Cohesive Segment Approach, J. Pipeline Syst. Eng. Pract. 11 (2020) 04020009. https://doi.org/10.1061/(ASCE)PS.1949-1204.0000444.

[44]   A. Okodi, Y. Li, R. Cheng, M. Kainat, N. Yoosef-Ghodsi, S. Adeeb, Crack Propagation and Burst Pressure of Pipeline with Restrained and Unrestrained Concentric Dent-Crack Defects Using Extended Finite Element Method, Appl. Sci. . 10 (2020). https://doi.org/10.3390/app10217554.

[45]   S. Agbo, A. Imanpour, Y. Li, M. Kainat, N. Yoosef-Ghodsi, J.J.R. Cheng, S. Adeeb, Development of a Tensile Strain Capacity Predictive Model for American Petroleum Institute 5L X42 Welded Vintage Pipelines, J. Press. Vessel Technol. 142 (2020). https://doi.org/10.1115/1.4047561.

[46]   J.H. Pan, Several concernment task under development of high strength pipeline steel,

Welded Pipe Tube. 28 (2005) 1–2.

[47]   M.L. Macia, S.A. Kibey, H. Arslan, F. Bardi, S.J. Ford, W.C. Kan, M.F. Cook, B. Newbury, Approaches to qualify strain-based designed pipelines, in: Proc. Bienn. Int. Pipeline Conf. IPC, American Society of Mechanical Engineers Digital Collection, Calgary, Canada, 2010: pp. 365–374. https://doi.org/10.1115/IPC2010-31662.

[48]   Y.Y. Wang, D. Rudland, R. Denys, D. Horsley, A preliminary strain-based design criterion for pipeline girth welds, in: Proc. Int. Pipeline Conf. IPC, American Society of Mechanical Engineers Digital Collection, 2002: pp. 415–427. https://doi.org/10.1115/IPC2002-27169.

[49]   Y.Y. Wang, W. Cheng, D. Horsley, Tensile strain limits of buried defects in pipeline girth welds, in: Proc. Bienn. Int. Pipeline Conf. IPC, American Society of Mechanical Engineers, 2004: pp. 1607–1614. https://doi.org/10.1115/ipc2004-0524.

[50]   Y. Wang, D. Horsley, W. Cheng, A. Glover, M. McLamb, J. Zhou, Tensile Strain Limits of Girth Welds with Surface-Breaking Defects Part II Experimental Correlation and Validation, Pipeline Technol. Proc. 4th Int. Conf. Pipeline Technol. (2004) 251–266.

[51]   S. Kibey, X. Wang, K. Minnaar, M.L. Macia, D.P. Fairchild, W.C. Kan, S.J. Ford, B. Newbury, Tensile Strain Capacity Equations for Strain-Based Design of Welded Pipelines, in: 2010 8th Int. Pipeline Conf. Vol. 4, ASME, 2010: pp. 355–363. https://doi.org/10.1115/IPC2010-31661.

[52]   D.P. Fairchild, S.A. Kibey, H. Tang, V.R. Krishnan, X. Wang, M.L. Macia, W. Cheng, Continued advancements regarding capacity prediction of strain-based pipelines, in: Proc.

Bienn. Int. Pipeline Conf. ASME Pap. No. IPC 2012-90471, American Society of
Mechanical Engineers Digital Collection, 2012: pp. 297–305.
https://doi.org/10.1115/IPC2012-90471.

[53]   H. Tang, D. Fairchild, M. Panico, J. Crapps, W. Cheng, Strain Capacity Prediction of
Strain-Based Pipelines, in: 2014 10th International Pipeline Conference, Calgary, Canada,
2014: p. V004T11A025. http://dx.doi.org/10.1115/IPC2014-33749.

[54]   Y.-Y. Wang, M. Liu, Y. Song, Second Generation Models for Strain-Based Design,
Pipeline Research Council International, 2011. https://rosap.ntl.bts.gov/view/dot/34533
(accessed August 10, 2020).

[55]   F.M. Rashid, A. Banerjee, Simulation of fracture in a low ductility aluminum alloy using a
triaxiality dependent cohesive model, Eng. Fract. Mech. 179 (2017) 1–12.
https://doi.org/https://doi.org/10.1016/j.engfracmech.2017.04.028.

[56]   C.-S. Oh, N.-H. Kim, Y.-J. Kim, J.-H. Baek, Y.-P. Kim, W.-S. Kim, A finite element
ductile failure simulation method using stress-modified fracture strain model, Eng. Fract.
Mech. 78 (2011) 124–137.
https://doi.org/https://doi.org/10.1016/j.engfracmech.2010.10.004.

[57]   X. Liu, H. Zhang, Y. Han, M. Xia, Y. Ji, Numerical and experimental study on critical
crack tip opening displacement of X80 pipeline steel, Mechanika. 23 (2017) 204–208.
https://doi.org/10.5755/j01.mech.23.2.14535.

[58]   D. Abdulhameed, C. Cakiroglu, M. Lin, R. Cheng, J. Nychka, M. Sen, S. Adeeb, The
Effect of Internal Pressure on the Tensile Strain Capacity of X52 Pipelines With

Circumferential Flaws, J. Press. Vessel Technol. 138 (2016) 61701. https://doi.org/10.1115/1.4033436.

[59] Abaqus 6.17, Documentation,2017. Dassault Systemes.

[60] G. Laschet, P. Fayek, T. Henke, H. Quade, U. Prahl, Derivation of anisotropic flow curves of ferrite-pearlite pipeline steel via a two-level homogenisation scheme, Mater. Sci. Eng. A. 566 (2013) 143–156. https://doi.org/10.1016/j.msea.2012.12.064.

[61] Y.M. Zhang, Z.M. Xiao, W.G. Zhang, On 3-D crack problems in offshore pipeline with large plastic deformation, Theor. Appl. Fract. Mech. 67–68 (2013) 22–28. https://doi.org/10.1016/j.tafmec.2014.01.001.

[62] D. Belato Rosado, W. De Waele, D. Vanderschueren, S. Hertelé, Latest developments in mechanical properties and metallurgical features of high strength line pipe steels, Int. J. Sustain. Constr. Des. 4 (2013). https://doi.org/10.21825/scad.v4i1.742.

[63] J.F. (Derick) Nixon, Thaw-Subsidence Effects on Offshore Pipelines, J. Cold Reg. Eng. 5 (1991) 28–39. https://doi.org/10.1061/(ASCE)0887-381X(1991)5:1(28).

[64] A.P.S. Selvadurai, S.B. Shinde, Frost Heave Induced Mechanics of Buried Pipelines, J. Geotech. Eng. 119 (1993) 1929–1951. https://doi.org/10.1061/(ASCE)0733-9410(1993)119:12(1929).

[65] A. Nobahar, S. Kenny, R. Phillips, Buried Pipelines Subject to Subgouge Deformations, Int. J. Geomech. 7 (2007) 206–216. https://doi.org/10.1061/(asce)1532-3641(2007)7:3(206).

[66]   H. Tang, M. Macia, K. Minnaar, P. Gioielli, S. Kibey, D. Fairchild, Development of the SENT test for strain-based design of welded pipelines, in: Proc. Bienn. Int. Pipeline Conf. IPC, American Society of Mechanical Engineers Digital Collection, 2010: pp. 303–312. https://doi.org/10.1115/IPC2010-31590.

[67]   Veritas DN, Fracture control for pipeline installation methods introducing cyclic plastic strain, in: 2006: pp. 1–24.

[68]   C. Soret, Y. Madi, J. Besson, V. Gaffard, Use of the sent specimen in pipeline design, in: 20th JTM-EPRG Eur. Pipeline Res. Gr., 2015: pp. 34-p.

[69]   A.R. Khoei, Extended Finite Element Method, John Wiley & Sons, Ltd, Chichester, UK, 2014. https://doi.org/10.1002/9781118869673.

[70]   S. Mohammadi, XFEM Fracture Analysis of Composites, John Wiley & Sons, Ltd, Chichester, UK, 2012. https://doi.org/10.1002/9781118443378.

[71]   X. Zhang, A. Okodi, L. Tan, J. Leung, S. Adeeb, Failure pressure prediction of cracks in corrosion defects using xfem, in: Proc. Bienn. Int. Pipeline Conf. IPC, American Society of Mechanical Engineers (ASME), 2020. https://doi.org/10.1115/IPC2020-9312.

[72]   N. Elyasi, M.. Shahzamanian, M. Lin, L. Westover, Y. Li, M. Kainat, N. Yoosef-Ghodsi, S. Adeeb, Prediction of Tensile Strain Capacity for X52 Steel Pipeline Materials Using the Extended Finite Element Method, Appl. Mech. 2 (2021) 209–225.

[73]   I. Ameli, B. Asgarian, M. Lin, S. Agbo, A. Imanpour, D.M. Duan, R. Cheng, S. Adeeb, Determination of CMOD-force curves and R-curves in side-grooved single edge notched

tensile (SENT) specimens in welded X42 pipeline steel, Int. J. Press. Vessel. Pip. 163 (2018) 68–74. https://doi.org/10.1016/j.ijpvp.2018.04.003.

[74]   I.S. ISO, 12135 Metallic materials--Unified method of test for the determination of quasistatic fracture toughness, Int. Organ. Stand. Geneva. (2007).

[75]   R. Dekker, F.P. Meer, J. Maljaars, L.J. Sluys, A cohesive XFEM model for simulating fatigue crack growth under mixed-mode loading and overloading, Int. J. Numer. Methods Eng. 118 (2019) 561–577. https://doi.org/10.1002/nme.6026.